

The complexity of dynamics in small neural circuits

Diego Fasoli^{1,*}, Anna Cattani¹, Stefano Panzeri¹

**1 Neural Computation Laboratory, Center for Neuroscience and Cognitive Systems
@Unitn, Istituto Italiano di Tecnologia, 38068 Rovereto (Tn), Italy**

* E-mail: diego.fasoli@iit.it

Abstract

Mean-field theory is a powerful tool for studying large neural networks. However, when the system is composed of a few neurons, macroscopic differences between the mean-field approximation and the real behavior of the network can arise. Here we introduce a study of the dynamics of a small firing-rate network with excitatory and inhibitory populations, in terms of local and global bifurcations of the neural activity. Our approach is analytically tractable in many respects, and sheds new light on the finite-size effects of the system. In particular, we focus on the formation of multiple branching solutions of the neural equations through spontaneous symmetry-breaking, since this phenomenon increases considerably the complexity of the dynamical behavior of the network. For these reasons, branching points may reveal important mechanisms through which neurons interact and process information, which are not accounted for by the mean-field approximation.

Author Summary

The mesoscopic scale represents the bridge between microscopic neural activity and the highest cognitive functions that emerge at the macroscopic level in the brain. For this reason, understanding the dynamics of small neural networks at this intermediate scale of organization is of fundamental importance. However, counter-intuitively, the behavior of small neural networks can be much more difficult to study mathematically than that of large networks. Here we introduce a finite-size firing-rate model and we study its local and global bifurcations by a combination of numerical and analytical techniques. This analysis shows the formation of strong and previously unexplored finite-size effects, that are particularly hard to detect in large networks. Their study advances the state of the art in the comprehension of neural circuits, beyond the results provided by the mean-field approximation and the techniques introduced so far for the quantification of finite-size effects.

1 Introduction

The structural complexity of the brain is reflected by its organization at multiple spatial scales [1]. At the highest level, the brain can be divided in macroscopic areas containing millions of neurons. These areas accomplish very complex roles, ranging from motor control to cognitive functions. On the opposite side, namely at the lowest level, the brain is made of its elementary blocks, the neurons, which provide a description of this complex organ at the microscopic scale. The level of spatial organization that lies between these macroscopic and microscopic pictures of the brain is called *mesoscopic scale*, and in the last years an increasing number of studies (e.g. [2–6]) have recognized its importance for the comprehension of the brain. This is the spatial scale that links the macroscopic and microscopic scales, and therefore that may explain how the highest cognitive functions arise from the cooperation and the exchange of

information between neurons. For this reason, finding an appropriate mathematical description of the brain at the mesoscopic scale is of fundamental importance for unveiling its emergent properties.

At the mesoscopic scale, the brain is often described as a collection of neural masses, i.e. homogeneous neuronal populations within a cortical column [7]. Usually, these groups of neurons are described by the so called *neural-mass models* [8]. A typical example is the well-known *Jansen-Rit model* [9–11], which describes a cortical minicolumn by a population of excitatory pyramidal cells, that receive inhibitory and excitatory feedback from local interneurons, and excitatory input from neighboring areas such as the thalamus. This model was originally intended to describe the formation of alpha rhythms within a cortical minicolumn of the visual cortex through the interaction of the excitatory and inhibitory populations, but provides only a coarse description of their dynamics. In [12] the authors proposed an improvement of the Jansen-Rit model based on the mean-field theory, which may provide a better understanding of MEG/EEG cortical recordings. The mean-field theory is a mathematical tool that approximates the behavior of large networks [13–15], and proves very convenient from the computational point of view since it describes the activity of large populations by means of a reduced number of equations, which are usually simpler to solve than the original network. This approximation becomes exact in the limit of networks with an infinite number of neurons, the so called *thermodynamic limit*. Clearly this means that for finite-size networks, the mean-field theory provides only an approximation of the real behavior of the system, and therefore may neglect important phenomena.

For example, in [16], for a class of random neural networks it was proved that in the thermodynamic limit the system undergoes a sharp transition from a static regime to chaos, while in the finite-size case this occurs gradually by a cascade of transitions that are not displayed by the mean-field approximation. Another important example is shown in [17], where the authors proved that a stochastic finite-size network can exhibit arbitrarily high levels of cross-correlations of the neural activity, while this phenomenon disappears when the size of the system grows to infinity. Clearly, these macroscopic differences in the dynamical and statistical behavior of finite and infinite-size networks may have important consequences on the information processing capability of the system. In other terms, the oversimplification of the mean-field approximation may hide important neural processes that are fundamental for the comprehension of the brain.

This explains the number of mathematical techniques that have been developed to quantify finite-size effects beyond the mean-field theory, such as the linear noise approximation [18], the density functional approach [19], large-deviations theory [20], path-integral methods [21], etc. Typically, these finite-size methods can be applied to networks composed of a finite but large number of neurons. However, neural masses in a cortical minicolumn contain only few tens of neurons since, according to different estimates [22–24], a minicolumn in primates contains about 80 – 100 neurons. Thus, for such small networks the mean-field description and the previously introduced techniques turn out to be inappropriate, since their finite-size effects can be relevant.

The analysis of the dynamics of small neural networks was started by Beer [25], who studied the bifurcations of networks of arbitrary size in highly symmetric cases, namely with rigid constraints on the strength of the synaptic weights. Through this analysis, he showed that small networks can exhibit complex dynamical behavior, which may have important neurobiological implications. In our article we extend his analysis to a more biologically plausible network of arbitrary size without specific conditions on the synaptic weights, and in particular we show another important difference between a finite-size network and its mean-field counterpart. In more detail, here we consider a deterministic finite-size firing-rate network model with excitatory and inhibitory populations composed of arbitrarily few neurons (we consider N_E neurons in the excitatory population and N_I neurons in the inhibitory one), which are indistinguishable within each population. Then, we perform a numerical analysis of the dynamics that emerge by varying the external input current to the network and the strength of inhibition, and we introduce a mathematical theory that allows us to describe local bifurcations analytically. In particular, we obtained macroscopic differences with the mean-field approximation when the system has strong

inhibitory synaptic weights. In this case, through a phenomenon of spontaneous symmetry-breaking, the neural network undergoes a special bifurcation known as *branching point* [26], from which multiple solutions of the neural equations emerge. On the new branches, new bifurcations can occur, enriching considerably the complexity of the bifurcation diagram of the neural network. For this reason, symmetry and branching points bifurcations may reveal important mechanisms through which neurons interact and process information, which are not accounted for by the mean-field approximation. Therefore a detailed analysis of their properties may be very important in order to understand the role of the mesoscopic scale in the emergence of brain’s highest functions.

It is important to observe that since we consider identical neurons within each population, our model lies in the context of the bifurcation theory of dynamical systems with symmetry, which is known as *equivariant bifurcation theory* [27]. This usually requires the reader to be familiar with advanced notions of group theory. Notwithstanding, here we follow a simpler approach, so the mathematical analysis introduced in this article is self-contained and accessible also to non-technical readers.

Symmetry-breaking and branching point bifurcations have already been studied in neuroscience through equivariant bifurcation theory, but in a conceptually different way. For example, in the theory of visual hallucinations developed by Ermentrout and Cowan [28], symmetry was used to evaluate hallucinations in primary visual cortex under the effect of drugs. They idealized the cortex as a plane and described the local activity of a population of neurons by means of neural field equations, so that each population is univocally identified by its position in the continuous space of the plane. Their theory exploits the symmetry the neural field equations inherit from the geometrically regular structure of the anatomical connections in primary visual cortex. In equivariant bifurcation theory, this symmetry is described by the invariance of the equations under the action of the Euclidean group $\mathbf{E}(2)$, which is the group of rigid motions in the plane, generated by translations, rotations, and reflections.

However, the network analyzed in our work is made of two populations containing a finite number of neurons, which are identified by a discrete index. In each population the neurons are identical, therefore the equations are symmetric under permutations of the neural indexes within a population. In more mathematical terms, our equations are invariant under the action of the group $S_{N_E} \times S_{N_I}$, where S_{N_α} is the permutation group on N_α items (also known as *symmetric group*). This is a completely different kind of symmetry compared to that of the Euclidean group $\mathbf{E}(2)$, and it allows us to study in an analytically simple way networks made of a finite number of neurons. Indeed, this is conceptually different from the theory of Ermentrout and Cowan, which relies on infinite-dimensional neural field equations. So their theory does not describe finite-size effects, and does not use the underlying symmetry for this purpose. In this respect, our theory is more similar to that developed in [29–32], where the authors exploited the invariance under the symmetric group S_N in a system with all-to-all coupling, and the subsequent spontaneous symmetry-breaking, as a possible mechanism to explain the origin of animal species. However, we are not aware of any application of this symmetry to the study of bifurcations in neural networks described by specific equations, such as Hopfield [33] or Wilson-Cowan [34] ones.

This article is organized as follows. In Sec. (2) we describe the neural model we use. Then we start Sec. (3) by explaining intuitively the main topic of this article, namely the formation of new branches of solutions through spontaneous symmetry-breaking, depending on the strength of inhibition (see SubSec. (3.1)). This is followed by a numerical and analytical study of the bifurcation points of the network in weak and strong-inhibition regimes (see SubSecs. (3.2) and (3.3) respectively). As we will see, the complexity of dynamics depends also on the size of the inhibitory population, therefore we start our analysis by showing the behavior of the network in the simplest case, namely $N_I = 2$, and then we explain how to generalize these results to a larger inhibitory population (see SubSec. (3.4)). We also show why the mean-field theory is an oversimplified description of the network (SubSec. (3.5)), and that the finite size effects studied in this work for a fully-connected network may be even stronger for more realistic topologies of the synaptic connections (SubSec. (3.6)). In Sec. (4) we examine the importance and the biological implications of our results. Finally, more details about the analytical calculations are

shown in Supplementary Materials.

2 Materials and Methods

The analysis of the dynamics of a neural network is a mathematically hard problem. Its complexity depends on the degree of biological plausibility of the system, which in turn is determined by:

- the variety of neural populations and realistic ratios between their sizes;
- the finite size of the network;
- the random behavior of the system;
- a realistic topology of the synaptic connections;
- plausible single-cell models for the soma and the synapse;
- delays in the transmission of the electric signals through the axons.

Among the points listed above, we select several biological plausible features that lead our model to be characterized by:

- two neural populations of excitatory and inhibitory neurons;
- a generic finite number of neurons in the network and in each population;
- non-symmetric and arbitrarily strong synaptic weights.

For the sake of clarity, in this article we perform a numerical and analytical analysis in the case of just two neural populations, since they are sufficient for describing dynamical behaviors, such as neural oscillations, which are thought to be at the base of fundamental cognitive processes. It is important to observe that our analysis can be extended to a generic number of neural populations, as we discuss briefly in SubSec. (S4.1) of the Supplementary Materials, but this problem will be addressed in more detail in another article. In order to make the analysis of the two-populations network analytically tractable, we make some simplifying assumptions that considerably reduce the complexity of the problem, without losing the most fundamental properties of a neural network:

- non-spiking neurons;
- identical neurons in each population;
- dense connections (i.e. fully-connected topology);
- absence of axonic delays;
- absence of random noise.

These features are supposed to not compromise the plausibility of the final result. Actually, this work is intended as a model of a neural mass within a cortical column, where neurons are homogeneous [7] and the density of the connections is known to be high, according to anatomical data (see for example [1]). This justifies the use of identical neurons in each populations and of a fully-connected topology. Moreover, since a single column is localized in a mesoscopic area of the brain, delays can be neglected. However, following [35,36], our analysis can be extended to the case of delay differential equations, if desired. Also random noise may be taken into account, as shown in [17], but this will be studied in detail in another article. To conclude, the choice of spiking or rate models is still under debate in the scientific community (see for example [37–40]) so this, together with the need for a mathematically tractable model, justifies our decision to work with a rate neural network.

In more detail, we consider a widely used model of rate network [7, 12, 15, 17, 25, 33]:

$$\frac{dV_i(t)}{dt} = -\frac{1}{\tau_i} V_i(t) + \frac{1}{M_i} \sum_{j=0}^{N-1} J_{ij} \mathcal{A}_j(V_j(t)) + I_i, \quad i = 0, \dots, N-1 \quad (1)$$

where $N \geq 2$ represents the number of neurons in the network. The function $V_i(t)$ is the membrane potential of the i th neuron, while τ_i is its membrane time constant. M_i , the total number of connections to the i th neuron, is a normalization factor that has been introduced to avoid the explosion of the total synaptic input $\sum_{j=0}^{N-1} J_{ij} \mathcal{A}_j(V_j(t))$ in equation (1) in the thermodynamic limit $N \rightarrow \infty$. The matrix J , also known as *structural* or *anatomical connectivity*, represents the specification of all the synaptic wirings that are physically present between neurons. It also quantifies the strength of these connections. So J_{ij} is the synaptic weight from the j th to the i th neuron, and for simplicity it is supposed to be deterministic and constant in time, for every pair of neurons. $\mathcal{A}_j(\cdot)$ is the activation function of the j th neuron and converts its membrane potential into the corresponding firing rate $\nu_j = \mathcal{A}(V_j)$. S -shaped (i.e. sigmoidal) activation functions are biologically plausible, however usually piecewise-linear functions are used in order to find analytical results [41–43]. In our work we show how it is possible to obtain analytical expressions for the equilibrium points and the local bifurcations of the network when $\mathcal{A}(V)$ is the so called *algebraic activation function*:

$$\mathcal{A}_j(V) = \frac{\nu_j^{\max}}{2} \left[1 + \frac{\frac{\Lambda_j}{2} (V - V_j^T)}{\sqrt{1 + \frac{\Lambda_j^2}{4} (V - V_j^T)^2}} \right] \quad (2)$$

Here ν^{\max} is the maximum firing rate, Λ determines the slope of the activation function when ν^{\max} is fixed, and V^T is the horizontal shift, so it can be interpreted as a firing threshold for the membrane potentials. In Eq. (1), I_i are external input currents, which in this article are supposed to be constant in time, in order to perform the bifurcation analysis of the network.

In order to make our analysis analytically tractable, we suppose that all the parameters of the system are indexed only at the population level. In other terms, within a given population, or between two fixed populations in the case of the synaptic weights, the parameters are homogeneous. If we define N_E (N_I) to be the size of the excitatory (inhibitory) population, and if we suppose that the neurons with indexes $i = 0, \dots, N_E - 1$ belong to the excitatory population, and those with $i = N_E, \dots, N - 1$ (with $N = N_E + N_I$) to the inhibitory one, this means that the synaptic connectivity matrix is structured as follows:

$$J = \begin{bmatrix} \mathfrak{J}_{EE} & \mathfrak{J}_{EI} \\ \mathfrak{J}_{IE} & \mathfrak{J}_{II} \end{bmatrix}, \quad \mathfrak{J}_{\alpha\beta} = \begin{cases} J_{\alpha\alpha} (\mathbb{I}_{N_\alpha} - \text{Id}_{N_\alpha}), & \text{for } \alpha = \beta \\ J_{\alpha\beta} \mathbb{I}_{N_\alpha, N_\beta}, & \text{for } \alpha \neq \beta \end{cases}$$

where the block $\mathfrak{J}_{\alpha\beta}$ is a $N_\alpha \times N_\beta$ matrix that represents the connections from the population β to the population α , with $\alpha, \beta \in \{E, I\}$. Moreover, $\mathbb{I}_{N_\alpha, N_\beta}$ is the $N_\alpha \times N_\beta$ all-ones matrix (here we use the simplified notation $\mathbb{I}_{N_\alpha} \stackrel{\text{def}}{=} \mathbb{I}_{N_\alpha, N_\alpha}$), while Id_{N_α} is the $N_\alpha \times N_\alpha$ identity matrix. Since, according to experimental measurements, about 80% of neocortical neurons are excitatory and the remaining 20% are inhibitory [44], in this article we consider $\frac{N_E}{N_I} = 4$. The zeros on the diagonal lines of the matrices \mathfrak{J}_{EE} and \mathfrak{J}_{II} are due to the absence of self-connections in biological networks. The real numbers J_{EE} ,

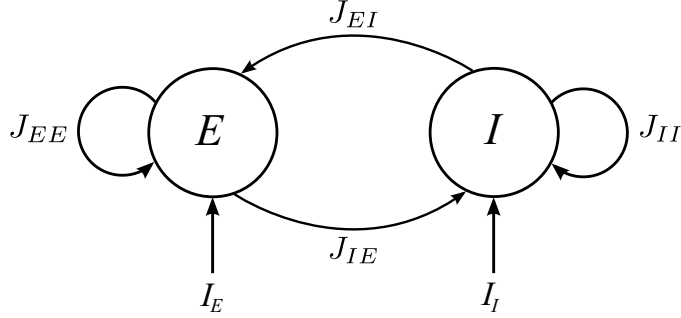


Figure 1: Structure of the network considered in this article.

J_{II} , J_{EI} , J_{IE} are free parameters that describe the strength of the interactions between and within the neural populations. Clearly we have $J_{EE}, J_{IE} > 0$, and $J_{II}, J_{EI} < 0$, which also means that $M_E = M_I = N - 1$. It is important to observe that, compared to [15], we have chosen a different normalization of the synaptic weights. In both the cases, the total synaptic input $\sum_{j=0}^{N-1} J_{ij} \mathcal{A}_j(V_j(t))$ is convergent in the thermodynamic limit, but they behave in different ways when the network is mixed with both finite-size and infinite-size populations. It is easy to check that according to our normalization, if one population has infinite size, then the contribution of the finite-size population in the total synaptic input goes to zero, which seems reasonable to us. On the other side, with the normalization introduced in [15], the infinite-size and finite-size populations both provide finite contributions to the total synaptic input. However, if required, it is possible to switch from our normalization to the other one by performing the following substitution:

$$J_{\alpha\beta} \rightarrow \frac{N-1}{N_\beta} J_{\alpha\beta}$$

in all the analytical results that we will obtain in the next sections and in the Supplementary Materials.

Moreover, from our assumption on the indexes, we obtain that the external input currents are divided in two vectors, \mathbf{I}_E and \mathbf{I}_I , namely the inputs to the excitatory and inhibitory populations. Clearly we get:

$$\mathbf{I}_\alpha = I_\alpha \mathbf{1}_{N_\alpha}$$

where $\mathbf{1}_{N_\alpha}$ is the $N_\alpha \times 1$ all-ones vector. Therefore the structure of the network is that shown in Fig. (1). The same subdivision between excitatory and inhibitory populations is performed for the other parameters of the network, namely τ , ν^{\max} , Λ , V_T .

To conclude, for the sake of clarity we observe that under our assumption on the neural indexes, we can rewrite the system (1) in the following explicit way:

$$\begin{cases} E: & \frac{dV_i(t)}{dt} = -\frac{1}{\tau_E} V_i(t) + \frac{J_{EE}}{N-1} \sum_{\substack{j=0 \\ j \neq i}}^{N_E-1} \mathcal{A}_E(V_j(t)) + \frac{J_{EI}}{N-1} \sum_{j=N_E}^{N-1} \mathcal{A}_I(V_j(t)) + I_E, & i = 0, \dots, N_E - 1 \\ I: & \frac{dV_i(t)}{dt} = -\frac{1}{\tau_I} V_i(t) + \frac{J_{IE}}{N-1} \sum_{j=0}^{N_E-1} \mathcal{A}_E(V_j(t)) + \frac{J_{II}}{N-1} \sum_{\substack{j=N_E \\ j \neq i}}^{N-1} \mathcal{A}_I(V_j(t)) + I_I, & i = N_E, \dots, N - 1 \end{cases} \quad (3)$$

Population Size	Synaptic Weights	Activation Functions	Other
$N_E = 8$	$J_{EE} = 10$	$\nu_E^{\max} = \nu_I^{\max} = 1$	$\tau_E = \tau_I = 1$
$N_I = 2$	$J_{EI} = -70$	$\Lambda_E = \Lambda_I = 2$	
	$J_{IE} = 70$	$V_E^T = V_I^T = 2$	

Table 1: Values of the parameters used in this article.

3 Results

The bifurcation analysis we perform provides an overview of the dynamics the model is able to exhibit, depending on two parameters: the static external currents $I_{E,I}$ in (3). In particular, we present this analysis for increasing values of a third parameter: the self-inhibition strength J_{II} . We focus on this parameter, instead of the other synaptic weights (i.e. J_{EE}, J_{EI}, J_{IE}), since J_{II} is directly responsible for the main phenomenon analyzed in this article, namely the formation of the branching point bifurcations. For the remaining synaptic weights we will provide only a qualitative description of the effects they exert on the system. The non-varying network parameters are chosen as in Tab. (1). In particular, we consider a network made of $N_E = 8$ excitatory neurons and $N_I = 2$ inhibitory ones, since we want to study finite-size effects in small neural masses.

We perform a detailed bifurcation analysis by means of numerical tools and, when possible, through analytical techniques. The numerical analysis is performed by exploiting the CLMatCont Matlab toolbox [45] and XPPAUT [46], that are grounded in the mathematical theory of bifurcations described in [26,47], while the analytical results are based on elementary methods from linear algebra. It is important to underline that bifurcations are defined by many conditions. Nonetheless, in our analytical study we checked only the conditions on the eigenvalues of the network, since they proved sufficient to reproduce the numerical results. Due to the high variety of the bifurcations the system exhibits, a rigorous check of all the remaining conditions is beyond the purpose of this article, and is left to the most technical readers.

3.1 Intuitive interpretation of the branching points

In mathematics, the branching point bifurcations are described by the so-called *equivariant bifurcation theory* [27], namely the study of bifurcations in symmetric systems. Being the latter rather technical, here we prefer to follow a more intuitive approach to the problem. So, first of all, we have to observe that according to bifurcation theory, local bifurcations are calculated by means of the eigenvalues of the Jacobian matrix of the network, evaluated at the equilibrium points. Therefore, we start by setting $\frac{dV_i(t)}{dt} = 0 \forall i$ in Eq. (3). The main observation of this article is that the system shows two different behaviors depending on the strength of J_{II} . As far as inhibition is weak (this will be quantified rigorously below), the equilibrium points in each population are homogeneous:

$$\boldsymbol{\mu} = \left(\overbrace{\mu_E, \dots, \mu_E}^{N_E\text{-times}}, \overbrace{\mu_I, \dots, \mu_I}^{N_I\text{-times}} \right) \quad (4)$$

where μ_E and μ_I are the solutions of the following system of algebraic non-linear equations, obtained from (3):

$$\begin{cases} \mathcal{F}(\mu_E, \mu_I) \stackrel{\text{def}}{=} -\frac{1}{\tau_E} \mu_E + \frac{N_E-1}{N-1} J_{EE} \mathcal{A}_E(\mu_E) + \frac{N_I}{N-1} J_{EI} \mathcal{A}_I(\mu_I) + I_E = 0 \\ \mathcal{G}(\mu_E, \mu_I) \stackrel{\text{def}}{=} -\frac{1}{\tau_I} \mu_I + \frac{N_E}{N-1} J_{IE} \mathcal{A}_E(\mu_E) + \frac{N_I-1}{N-1} J_{II} \mathcal{A}_I(\mu_I) + I_I = 0 \end{cases} \quad (5)$$

The curves defined by Eqs. $\mathcal{F}(x, y) = 0$ and $\mathcal{G}(x, y) = 0 \forall (x, y) \in \mathbb{R}^2$ are the so called *nullclines* of the network. Fig. (2) (top) shows an example obtained for $J_{II} = -10$, while the remaining parameters are chosen as in Tab. (1). In Sec. (S2) of the Supplementary Materials we show how to get approximate analytical solutions for $\mu_{E,I}$.

From (5), we can see that the Jacobian matrix \mathcal{J} of the network on the primary branch of solutions (4) is:

$$\mathcal{J} = \begin{bmatrix} \mathcal{J}_{EE} & \mathcal{J}_{EI} \\ \mathcal{J}_{IE} & \mathcal{J}_{II} \end{bmatrix}, \quad \mathcal{J}_{\alpha\beta} = \begin{cases} -\frac{1}{\tau_\alpha} \text{Id}_{N_\alpha} + \frac{J_{\alpha\alpha}}{N-1} \mathcal{A}'_\alpha(\mu_\alpha) (\mathbb{I}_{N_\alpha} - \text{Id}_{N_\alpha}), & \text{for } \alpha = \beta \\ \frac{J_{\alpha\beta}}{N-1} \mathcal{A}'_\beta(\mu_\beta) \mathbb{I}_{N_\alpha, N_\beta}, & \text{for } \alpha \neq \beta \end{cases} \quad (6)$$

therefore we can prove (see SubSec. (S3.1) of the Supplementary Materials) that its eigenvalues are:

$$\lambda_{0,1} = \frac{\delta + \eta \pm \sqrt{(\delta - \eta)^2 + 4\gamma}}{2}, \quad \lambda_E = -\left[\frac{1}{\tau_E} + \frac{J_{EE}}{N-1} \mathcal{A}'_E(\mu_E) \right], \quad \lambda_I = -\left[\frac{1}{\tau_I} + \frac{J_{II}}{N-1} \mathcal{A}'_I(\mu_I) \right] \quad (7)$$

where:

$$\delta = -\frac{1}{\tau_E} + \frac{N_E-1}{N-1} J_{EE} \mathcal{A}'_E(\mu_E), \quad \eta = -\frac{1}{\tau_I} + \frac{N_I-1}{N-1} J_{II} \mathcal{A}'_I(\mu_I), \quad \gamma = \frac{N_E N_I}{(N-1)^2} J_{EI} J_{IE} \mathcal{A}'_E(\mu_E) \mathcal{A}'_I(\mu_I) \quad (8)$$

According to bifurcation theory, the system undergoes special bifurcations when one of its eigenvalues is equal to zero. In particular, the branching point bifurcations are given by the condition $\lambda_I = 0$, so this allows us to define the weak and strong-inhibition regimes quantitatively by the conditions $\lambda_I < 0$ and $\lambda_I \geq 0$, respectively.

When the network undergoes a branching point bifurcation, we observe the formation of heterogeneous membrane potentials in the inhibitory population: in other terms, under strong inhibition the symmetry of the system is broken. Intuitively, this can be understood as in Fig. (3). When $|J_{II}|$ is small, there is only one valley or basin in the “energy landscape” of the network. On the other side, for strong inhibition we observe the formation of multiple valleys, and a small perturbation determines to which one the inhibitory potential will converge. For this reason, now multiple new branches of the equilibrium points emerge, which are described by the following stationary solutions:

$$\boldsymbol{\mu} = \left(\overbrace{\mu_E, \dots, \mu_E}^{N_E\text{-times}}, \mu_{I,0}, \dots, \mu_{I,N_I-1} \right) \quad (9)$$

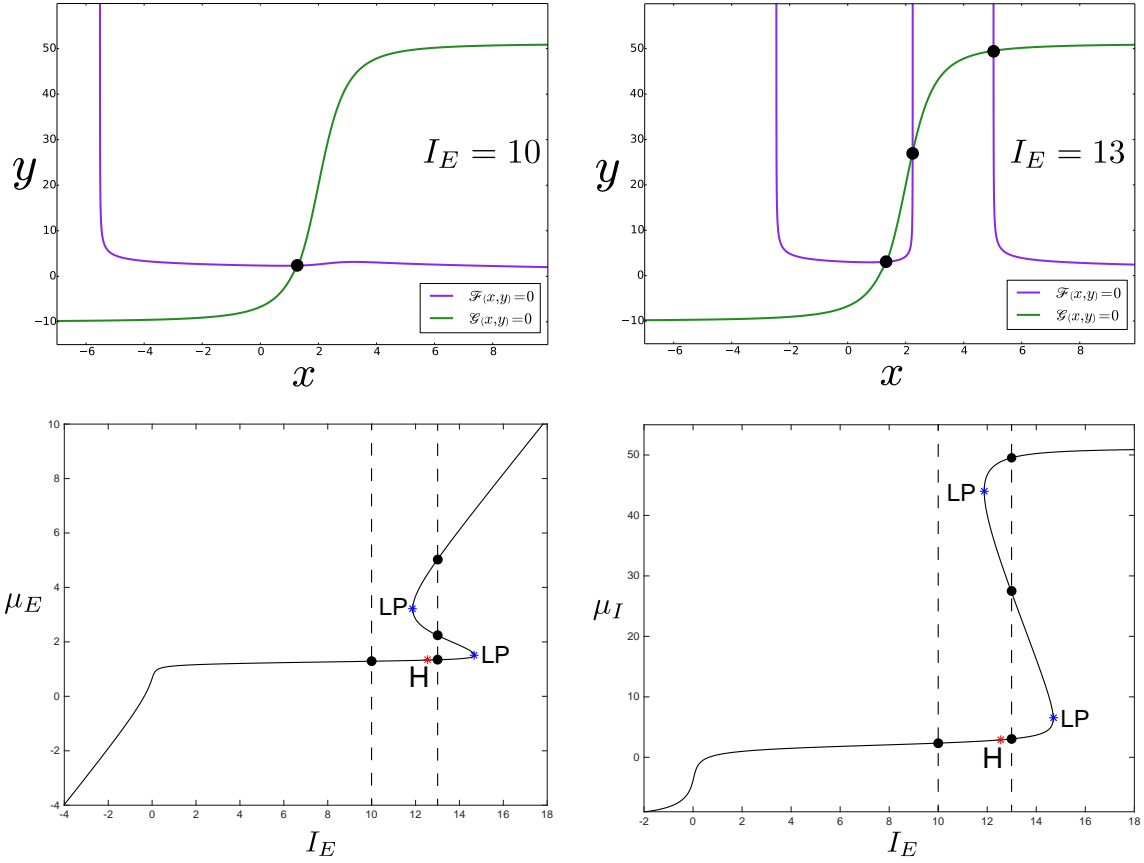


Figure 2: The two figures on the top show the nullclines of the network for fixed values of $I_{E,I}$ in a weak-inhibition regime, obtained for $J_{II} = -10$ and the values of the parameters in Tab. (1). Their intersection points (black dots) correspond to the solutions of the system (5). The top-left figure was obtained for $I_E = 10$, $I_I = -10$, while the top-right figure for $I_E = 13$, $I_I = -10$. Clearly the system (5) admits multiple solutions for specific values of the parameters. The two figures at the bottom show the solutions μ_E and μ_I (bottom-left and bottom-right panel, respectively) of the system (5) for the same values of the parameters, but with varying current I_E . The black curve represents the primary branch of the network equations, and for $I_E = 10$ and $I_E = 13$ it admits one and three solutions respectively (see the black dots at the intersection with the vertical dashed lines). The (μ_E, μ_I) coordinates of these solutions correspond to those of the black dots in the top panels of the figure. Here we do not care about the stability of the solutions, which is shown for the sake of completeness in Fig. (S5) of the Supplementary Materials.

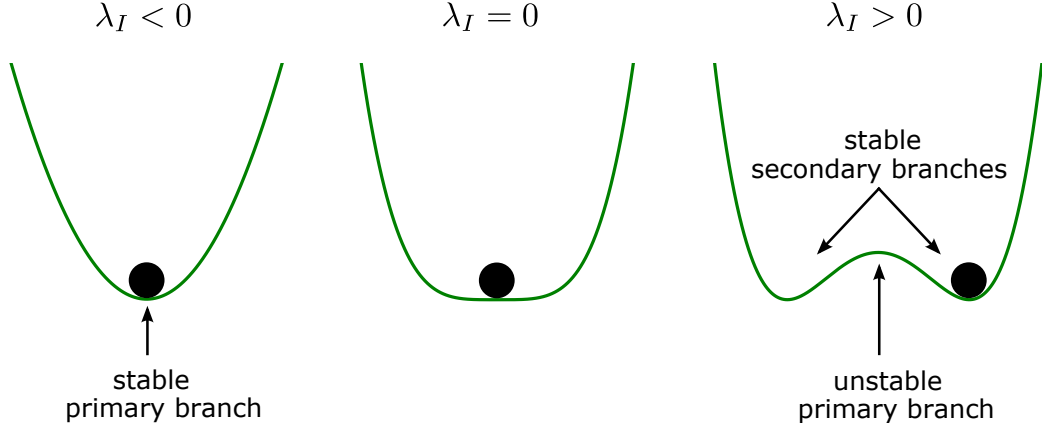


Figure 3: Spontaneous symmetry-breaking. For weak inhibition, the eigenvalue λ_I (see Eq. (7)) is negative, and the system (3) has only one stationary solution. This solution is stable and symmetric, but for increasing inhibition λ_I changes sign, therefore the solution becomes unstable and the network chooses randomly between two new alternative stable states, breaking the symmetry. This phenomenon can be understood intuitively by means of a ball that rolls in a double well potential in order to reach a state of minimum energy, that we interpret as a stable stationary solution of Eq. (3).

where μ_E and $\mu_{I,i}$ are the solutions of the following system of algebraic non-linear equations, obtained from (3) in the stationary regime:

$$\begin{cases} -\frac{1}{\tau_E}\mu_E + \frac{N_E-1}{N-1}J_{EE}\mathcal{A}_E(\mu_E) + \frac{J_{EI}}{N-1}\sum_{j=0}^{N_I-1}\mathcal{A}_I(\mu_{I,j}) + I_E = 0 \\ -\frac{1}{\tau_I}\mu_{I,i} + \frac{N_E}{N-1}J_{IE}\mathcal{A}_E(\mu_E) + \frac{J_{II}}{N-1}\sum_{\substack{j=0 \\ j \neq i}}^{N_I-1}\mathcal{A}_I(\mu_{I,j}) + I_I = 0 \quad \text{for } i = 0, \dots, N_I - 1 \end{cases} \quad (10)$$

For example, for $N_I = 2$ Eq. (10) can be written more explicitly as follows:

$$\begin{cases} \mathcal{F}(\mu_E, \mu_{I,0}, \mu_{I,1}) \stackrel{\text{def}}{=} -\frac{1}{\tau_E}\mu_E + \frac{N_E-1}{N-1}J_{EE}\mathcal{A}_E(\mu_E) + \frac{J_{EI}}{N-1}[\mathcal{A}_I(\mu_{I,0}) + \mathcal{A}_I(\mu_{I,1})] + I_E = 0 \\ \mathcal{G}(\mu_E, \mu_{I,0}, \mu_{I,1}) \stackrel{\text{def}}{=} -\frac{1}{\tau_I}\mu_{I,0} + \frac{N_E}{N-1}J_{IE}\mathcal{A}_E(\mu_E) + \frac{J_{II}}{N-1}\mathcal{A}_I(\mu_{I,1}) + I_I = 0 \\ \mathcal{H}(\mu_E, \mu_{I,0}, \mu_{I,1}) \stackrel{\text{def}}{=} -\frac{1}{\tau_I}\mu_{I,1} + \frac{N_E}{N-1}J_{IE}\mathcal{A}_E(\mu_E) + \frac{J_{II}}{N-1}\mathcal{A}_I(\mu_{I,0}) + I_I = 0 \end{cases} \quad (11)$$

The surfaces $\mathcal{F}(x, y, z) = 0$, $\mathcal{G}(x, y, z) = 0$, $\mathcal{H}(x, y, z) = 0 \forall (x, y, z) \in \mathbb{R}^3$ are a higher-dimensional extension of the nullclines $\mathcal{F}(x, y) = 0$ and $\mathcal{G}(x, y) = 0 \forall (x, y) \in \mathbb{R}^2$ that we encountered in the weak-inhibition regime. Sometimes they are called *nullsurfaces* (see for example [25]). Fig. (4) (top) shows an example obtained for $J_{II} = -100$, while the remaining parameters are chosen as in Tab. (1).

For the sake of clarity, here we treat in detail only the case $N_I = 2$, while we will show some results for $N_I > 2$ in SubSec. (3.4). So, for $N_I = 2$, from Eq. (11) we get that the Jacobian matrix on the secondary branches (9) is:

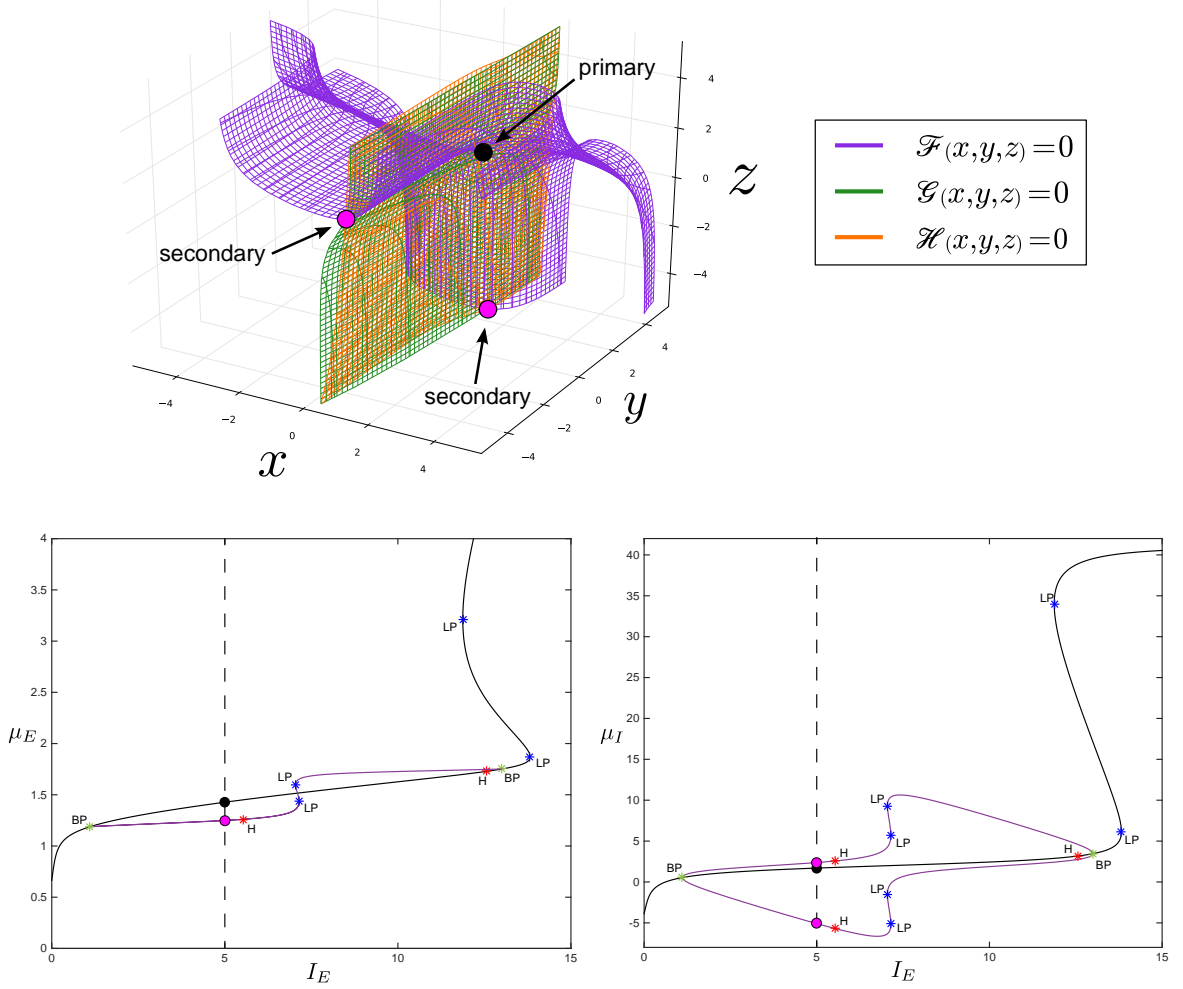


Figure 4: The figure on the top shows the nullsurfaces of the network for fixed values of $I_{E,I}$ in a strong-inhibition regime, obtained for $J_{II} = -100$, $I_E = 5$, $I_I = -10$ and the values of the parameters in Tab. (1). The black intersection point corresponds to the solution of the system (11) on the primary branch, while the purple dots represent the solutions on the secondary branches. The two figures at the bottom show the solutions μ_E and μ_I (left and right panel, respectively) of the system (11) for the same values of the parameters, but with varying current I_E . The black and violet curves represent respectively the primary and secondary branches of the network equations. For $I_E = 5$ the system admits three solutions (μ_E, μ_I) (see the dots at the intersection with the vertical dashed lines: we have just three solutions because μ_I has three intersection points, two of which, i.e. the pink ones in the right panel, correspond to the same μ_E , i.e. the pink dot in the left panel). The (μ_E, μ_I) coordinates of these solutions correspond to those of the dots in the top panel of the figure. Again, here we do not care about the stability of the solutions, which is shown for the sake of completeness in Fig. (9) and in Fig. (S9) of the Supplementary Materials.

$$\mathcal{J} = \begin{bmatrix} \mathcal{J}_{00} & \mathcal{J}_{01} & \mathcal{J}_{02} \\ \mathcal{J}_{10} & \mathcal{J}_{11} & \mathcal{J}_{12} \\ \mathcal{J}_{20} & \mathcal{J}_{21} & \mathcal{J}_{22} \end{bmatrix} \quad (12)$$

where:

$$\mathcal{J}_{00} = -\frac{1}{\tau_E} \text{Id}_{N_E} + \frac{J_{EE}}{N-1} \mathcal{A}'_E(\mu_E) (\mathbb{I}_{N_E} - \text{Id}_{N_E}), \quad \mathcal{J}_{01} = \frac{J_{EI}}{N-1} \mathcal{A}'_I(\mu_{I,0}) \mathbf{1}_{N_E}, \quad \mathcal{J}_{02} = \frac{J_{EI}}{N-1} \mathcal{A}'_I(\mu_{I,1}) \mathbf{1}_{N_E},$$

$$\mathcal{J}_{10} = \frac{J_{IE}}{N-1} \mathcal{A}'_E(\mu_E) \mathbf{1}_{N_E}^T, \quad \mathcal{J}_{11} = \frac{1}{\tau_I}, \quad \mathcal{J}_{12} = \frac{J_{II}}{N-1} \mathcal{A}'_I(\mu_{I,1}),$$

$$\mathcal{J}_{20} = \frac{J_{IE}}{N-1} \mathcal{A}'_E(\mu_E) \mathbf{1}_{N_E}^T, \quad \mathcal{J}_{21} = \frac{J_{II}}{N-1} \mathcal{A}'_I(\mu_{I,0}), \quad \mathcal{J}_{22} = \frac{1}{\tau_I}$$

(here T is the transpose of a matrix), as explained in more detail in SubSec. (S4.1) of the Supplementary Materials. Intuitively, on the primary branch the Jacobian matrix was a 2×2 block matrix (see Eq. (6)), because we had only an excitatory and an inhibitory membrane potential (μ_E and μ_I respectively), while on the secondary branch it is a 3×3 block matrix, because now the two inhibitory neurons have different potentials ($\mu_{I,0}$ and $\mu_{I,1}$). The Jacobian matrix on the new branches can be calculated for a network with a generic number of inhibitory neurons (see the Supplementary Materials for more details).

Finally, we observe that it is possible to find relations between the inhibitory membrane potentials in the strong-inhibition regime, which prove very useful when we calculate analytically the local bifurcations of the system. For example, in the case $N_I = 2$, from the second and third equation of the system (11), after some algebra we get the following forth-order polynomial equation:

$$\widehat{a}\mu_{I,1}^4 + \widehat{b}\mu_{I,1}^3 + \widehat{c}\mu_{I,1}^2 + \widehat{d}\mu_{I,1} + \widehat{e} = 0 \quad (13)$$

whose coefficients depend on $\mu_{I,0}$ as follows:

$$\begin{aligned}
\hat{a} &= \frac{\Lambda_I^2}{4\tau_I^2} \\
\hat{b} &= -\frac{\Lambda_I^2}{2\tau_I} \left(\hat{\psi} + \frac{V_I^T}{\tau_I} \right) \\
\hat{c} &= \frac{\Lambda_I^2}{4} \left[\hat{\psi}^2 + \left(\frac{V_I^T}{\tau_I} \right)^2 + \frac{4}{\tau_I} V_I^T \hat{\psi} \right] + \frac{1}{\tau_I^2} - \hat{\xi} \\
\hat{d} &= -\frac{\Lambda_I^2}{2} \hat{\psi} V_I^T \left(\frac{V_I^T}{\tau_I} + \hat{\psi} \right) - \frac{2}{\tau_I} \hat{\psi} + 2\hat{\xi} V_I^T \\
\hat{e} &= \left(\frac{\Lambda_I}{2} \hat{\psi} V_I^T \right)^2 + \hat{\psi}^2 - \hat{\xi} (V_I^T)^2 \\
\hat{\psi} &= \frac{1}{\tau_I} \mu_{I,0} + \frac{J_{II}}{N-1} \mathcal{A}_I(\mu_{I,0}) - \frac{\nu_I^{\max} J_{II}}{2(N-1)} \\
\hat{\xi} &= \left(\frac{\nu_I^{\max} \Lambda_I J_{II}}{4(N-1)} \right)^2
\end{aligned}$$

Eq. (13) can be solved analytically, providing an explicit expression of $\mu_{I,1}$ as a function of $\mu_{I,0}$, which will be used in SubSec. (3.3) to evaluate the local bifurcations in the strong-inhibition regime.

3.2 Weak-inhibition regime ($\lambda_I < 0$)

As we said, we want to understand how the network's dynamics changes when we vary the external input currents $I_{E,I}$ and the strength of the synaptic weight J_{II} . For the sake of clarity, in this section we show the results that we obtain when we vary these parameters one by one, because this allows us to introduce the concepts of codimension one and codimension two bifurcation diagrams.

We start by considering fixed $I_{E,I}$ and inhibitory strength $J_{II} = -10$. As we can see from Fig. (2) (top), Eq. (5) admits multiple solutions, depending on the specific value that we have chosen for the current I_E . Then, we start to vary I_E continuously, while keeping I_I and J_{II} fixed. In this way we can plot how the solutions $\mu_{E,I}$ of the system (5) change as a function of I_E . As we anticipated in SubSec. (3.1), the curve that we obtain is called the *primary branch* of the network, see Fig. (2) (bottom). This figure represents the *codimension one bifurcation diagram* of the network, from which we see there are two special points, called *local saddle-node bifurcations*, or LP for short. They identify the value of I_E for which the number of solutions of Eq. (5) changes (notice the correspondence with the top panels of Fig. (2)). These are the first example of (local) bifurcation points that the neural network exhibits, and that lead to the formation of hysteresis (see the left panel in Fig. (5)). Hysteresis was suggested to describe short-term memory, since a sufficiently strong input can lead the system to reach a stable-high level of activity that is maintained when the input is turned off [48–50]. This phenomenon, known as *reverberation*, namely the persistence of neural activity sustained internally in the brain after a stimulus is removed, can be achieved through bistability, which can be present intrinsically at the single cell level or generated by recurrent excitatory connections. A typical example is the working memory, which is intimately related to the prefrontal cortex and that can retain information for a time span of the order

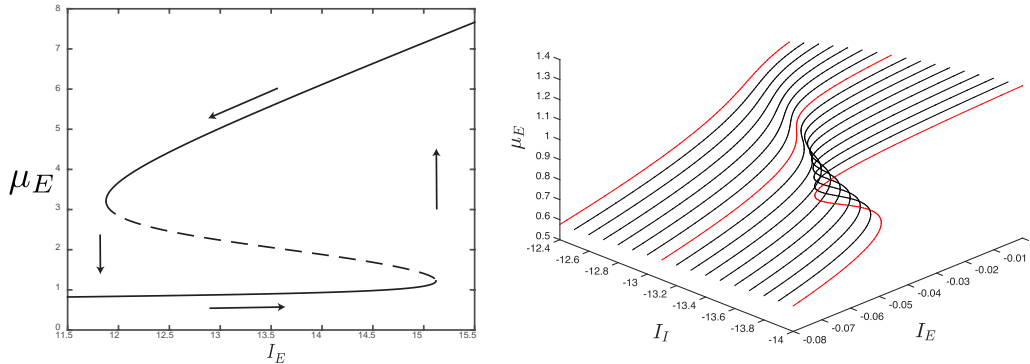


Figure 5: On the left, we show an example of hysteresis displayed by the system. The plain lines describe stable equilibria, while the dashed line the unstable ones. On the right, we show an example of catastrophe manifold. The panel highlights three different behaviors of the network for increasing values of $|I_I|$: leaky integrator, perfect integrator and switch (red curves). The readers are referred to [54, 55] for more details about their biological relevance.

of seconds, before it is erased by events such as noise or distracting stimuli. It is important to observe that even if reverberation requires bistability, the latter can be present without hysteresis, but very often they coexist, as in our model.

If now we continuously vary both I_E and I_I , while keeping J_{II} fixed, we can plot the solutions of Eq. (5) as a function of both the external currents, so now $\mu_{E,I} = \mu_{E,I}(I_E, I_I)$ define three dimensional manifolds (see Fig. (6) for μ_E). On these manifolds, the special points LP depend also on I_I , therefore they form a set of points called *saddle-node curves* (see the blue curves in Fig. (6)). For visual convenience, these curves are projected on the $I_E - I_I$ plane (see Fig. (7)), defining the so-called *codimension two bifurcation diagram* of the network (which is, from the analytical point of view, our main interest in this article, while the codimension one diagram is partially calculated in Sec. (S2) of the Supplementary Materials). However, from Fig. (6) and the bottom panels of Fig. (2), we can see that the saddle-nodes are not the only bifurcations we have in our network. For some values of the pair $I_E - I_I$, the system can undergo also a so called *local Andronov-Hopf bifurcation*, or H for short. These bifurcations are represented by the red curves in Figs. (6) and (7), and correspond to the emergence of neural oscillations, which are thought to play a key role in many cognitive processes [51].

Hereafter, we list all the bifurcations the system undergoes, dividing them in groups depending on the codimension of the bifurcation, which is defined as the number of parameters (in our case $I_{E,I}$) that must be varied for the bifurcation to occur. Although only few of them are represented in Fig. (2), the complete set of codimension one bifurcations our system undergoes is:

- local saddle-node bifurcations (LP), for which new equilibria arise, or collide and annihilate each other;
- local Andronov-Hopf bifurcations (H), where stable or unstable self-sustained oscillations, described by limit cycles, arise or disappear;
- global homoclinic bifurcations, where limit cycles vanish in a particular equilibrium point (i.e. a neutral saddle, see SubSec. (3.3), or a saddle-node), giving rise to an orbit with infinite period;
- global limit point of cycles bifurcations, at which new limit cycles arise, or collide and annihilate each other.

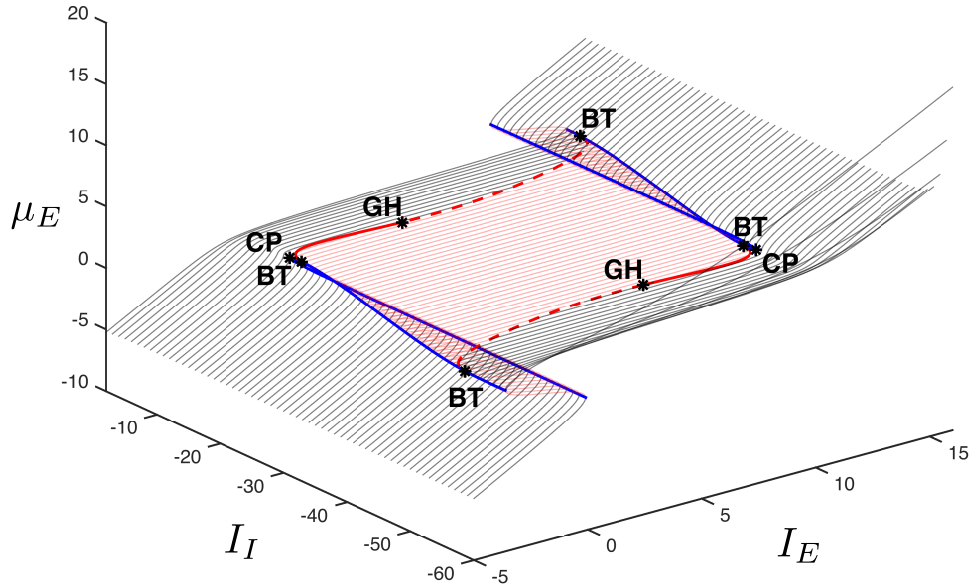


Figure 6: Three-dimensional bifurcation diagram equivalent to that in Fig. (7). The values of μ_E are shown on the z -axis as functions of $I_E - I_I$. Here we plot only the local bifurcations (blue: saddle-node curves, red: Andronov-Hopf curves) that bound the gray/red regions representing the stable/unstable equilibrium point areas. All the codimension two bifurcations are reported in Fig. (7).

The codimension one diagrams collecting all these bifurcations are shown in Fig. (S5) of the Supplementary Materials. Moreover, on the curves defined by these bifurcations, and that are obtained by varying both I_E and I_I , the following codimension two bifurcations appear (see Fig. 7):

- local cusp bifurcations (CP), on the saddle-node curves;
- local generalized Hopf bifurcations (GH), that divide subcritical Andronov-Hopf curves from supercritical ones;
- local Bogdanov-Takens bifurcations (BT), that represent the contact point between the saddle-node, Andronov-Hopf (ending here) and homoclinic curves;
- global cusp of limit point of cycles (CPC), on the limit point of cycles curves;
- global saddle-node on invariant circle (SNIC), where a saddle-node bifurcation occurs simultaneously with a homoclinic bifurcation.

It is worth remarking that the bifurcation diagram in Fig. (7), obtained from the voltage-based model (3) in the weak-inhibition regime, is qualitatively similar to that of the activity-based Wilson-Cowan model (see Fig. 2.12 in [52]). These two kinds of models are obtained from neural mass equations through two slightly different hypothesis about the postsynaptic potentials [7]. For this reason, in the literature it has always been assumed implicitly that the two models can exhibit qualitatively similar dynamics. The strong resemblance of their codimension two bifurcation diagrams proved in this article confirms rigorously this intuition (notwithstanding, in the next section we will show that things may change significantly in the strong-inhibition regime if we take into account finite-size effects).

Interestingly, Fig. (6) presents two of the so-called *catastrophe manifolds* [53], one of which is shown in the right panel of Fig. (5). This figure emphasizes the ability of the model to describe three different

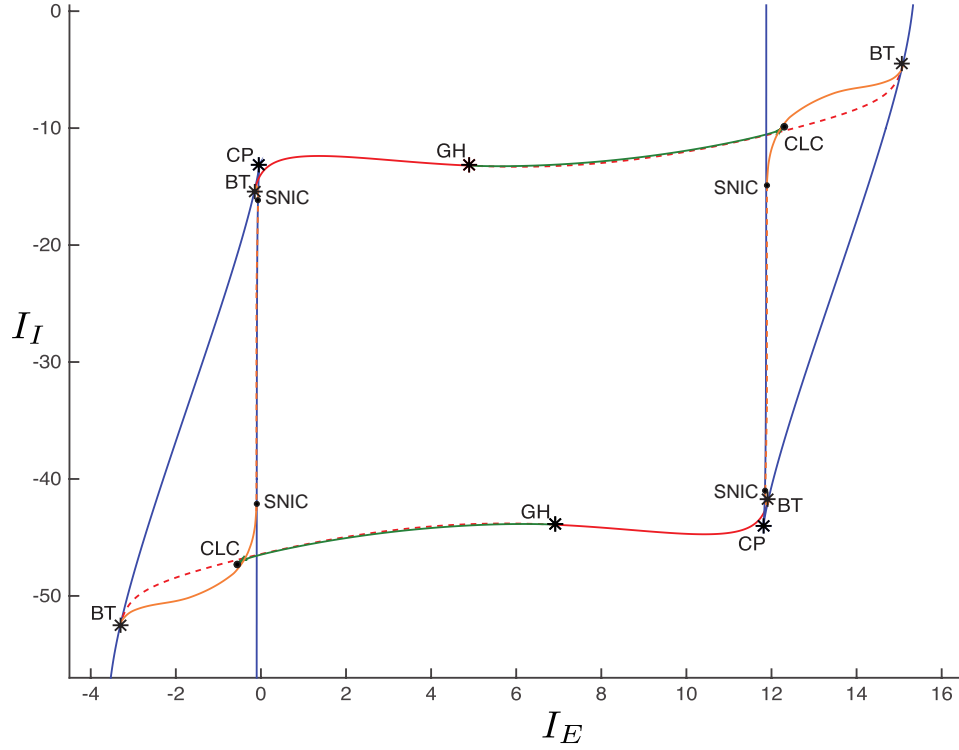


Figure 7: Complete codimension two bifurcation diagram on the $I_E - I_I$ plane in the weak-inhibition regime. The Andronov-Hopf bifurcation curves (red lines) are divided into supercritical (plain) and subcritical (dashed) portions. The supercritical/subcritical portions are bounded by a Generalized Hopf bifurcation, GH, and Bogdanov-Takens bifurcations, BT. The latter are the contact points among saddle-node bifurcation curves (blue lines), Andronov-Hopf bifurcation curves (red lines), and homoclinic bifurcation curves (hyperbolic-saddle/saddle-node homoclinic bifurcations are described by plain/dashed orange curves). SNIC bifurcations identify the contact point between the saddle-node curve and the homoclinic one. From GH originate two Limit Point of Cycles curves (dark green lines) that collapse into the homoclinic curves. Before this, they present a cusp bifurcation, CLC. Each saddle-node curve shows, in addition to BT, a cusp bifurcation, CP.

behaviors: leaky integrator, perfect integrator and switch. This triad represents the main ingredient for describing a mechanism which was proposed to explain interval timing by neural integration [54, 55]. According to the theory, by changing some parameters of the network, it is possible to modify the shape of the equilibrium curve on the catastrophe manifold, generating a ramping activity that can explain Weber's law of time perception [56]. This phenomenon can easily occur in our model, where the shape of the equilibrium curve can be changed dynamically by varying the input currents.

Now we want to prove some of our previous results on bifurcations from the analytical point of view. Often, in dynamical systems, global bifurcations are harder to study analytically, therefore here we focus on LP, H and BT. So first of all we observe that, according to bifurcation theory [26, 47], LP is mathematically defined by the condition that one real eigenvalue of the Jacobian matrix becomes equal to zero. Therefore, from Eq. (7), we conclude that for our network this bifurcation occurs whenever $\lambda_0 = 0$ or $\lambda_1 = 0$, because λ_E is always negative, while $\lambda_I = 0$ defines the branching point bifurcation. For example, if $\delta + \eta < 0$, the condition $\lambda_0 = 0$ is equivalent to $\delta\eta = \gamma$ which, according to Eq. (8), provides:

$$\mathcal{A}'_I(\mu_I) = \frac{-\frac{1}{\tau_E \tau_I} + \frac{1}{\tau_I} \frac{N_E - 1}{N - 1} J_{EE} \mathcal{A}'_E(\mathbf{v})}{-\frac{1}{\tau_E} \frac{N_I - 1}{N - 1} J_{II} + \frac{1}{(N - 1)^2} [(N_E - 1)(N_I - 1) J_{EE} J_{II} - N_E N_I J_{EI} J_{IE}] \mathcal{A}'_E(\mathbf{v})} \quad (14)$$

where we have defined the parameter $\mathbf{v} \stackrel{\text{def}}{=} \mu_E$. Now we invert $\mathcal{A}'_I(\mu_I)$ (more details are provided in SubSec. (S3.2.1) of the Supplementary Materials), obtaining:

$$\mu_I(\mathbf{v}) = V_I^T \pm \frac{2}{\Lambda_I} \sqrt{\sqrt[3]{\left(\frac{\nu_I^{\max} \Lambda_I}{4 \mathcal{A}'_I(\mu_I)}\right)^2} - 1} \quad (15)$$

and from Eq. (5) we get:

$$\begin{cases} I_E(\mathbf{v}) = \frac{1}{\tau_E} \mathbf{v} - \frac{N_E - 1}{N - 1} J_{EE} \mathcal{A}_E(\mathbf{v}) - \frac{N_I}{N - 1} J_{EI} \mathcal{A}_I(\mu_I(\mathbf{v})) \\ I_I(\mathbf{v}) = \frac{1}{\tau_I} \mu_I(\mathbf{v}) - \frac{N_E}{N - 1} J_{IE} \mathcal{A}_E(\mathbf{v}) - \frac{N_I - 1}{N - 1} J_{II} \mathcal{A}_I(\mu_I(\mathbf{v})) \end{cases} \quad (16)$$

These are parametric equations in the parameter $\mathbf{v} \in (\mathbf{v}_a, \mathbf{v}_b)$, where:

$$\mathbf{v}_{b,a} = V_E^T \pm \frac{2}{\Lambda_E} \sqrt{\sqrt[3]{\left(\frac{N_E - 1}{N - 1} J_{EE} \frac{\nu_E^{\max} \Lambda_E}{4 \tau_E}\right)^2} - 1} \quad (17)$$

and they define analytically the blue curves in Fig. (7). As we said, this is not sufficient to prove that Eqs. (14) - (17) describe saddle-node curves, since we should check also the corresponding non-degeneracy conditions. Nevertheless, we observe a perfect agreement between these analytical curves and those obtained numerically by Cl.MatCont and XPPAUT, therefore for simplicity we do not check the remaining conditions and we leave them to the most technical readers. We adopt the same approach for the remaining bifurcations we are about to describe.

Now we focus on the H bifurcations. According to [26, 47], they appear whenever the network has conjugate purely imaginary eigenvalues. Since $\lambda_{E,I}$ are always real, this condition can be satisfied only by $\lambda_{0,1}$, by setting $\delta + \eta = 0$ and $(\delta - \eta)^2 + 4\gamma < 0$. In particular, from the equation $\delta + \eta = 0$ we get:

$$\mathcal{A}'_I(\mu_I) = \frac{N-1}{(N_I-1)J_{II}} \left[\frac{1}{\tau_E} + \frac{1}{\tau_I} - \frac{N_E-1}{N-1} J_{EE} \mathcal{A}'_E(\mathbf{v}) \right] \quad (18)$$

where $\mathbf{v} \stackrel{\text{def}}{=} \mu_E$ as before. Following the same procedure introduced before for the LP curves, we obtain a set of parametric equations for the pairs $I_E - I_I$ that generate the H curves, with parameter $\mathbf{v} \in [\mathbf{v}_f, \mathbf{v}_d] \cup [\mathbf{v}_c, \mathbf{v}_e]$, where:

$$\begin{aligned} \mathbf{v}_{c,d} &= V_E^T \pm \frac{2}{\Lambda_E} \sqrt[3]{\sqrt{\left(\frac{\nu_E^{\max} \Lambda_E (N_E - 1) J_{EE}}{4(N-1)} \frac{1}{\frac{1}{\tau_E} + \frac{1}{\tau_I} - \frac{\nu_I^{\max} \Lambda_I (N_I - 1) J_{II}}{4(N-1)}} \right)^2} - 1} \\ \mathbf{v}_{e,f} &= V_E^T \pm \frac{2}{\Lambda_E} \sqrt[3]{\left(\frac{\nu_E^{\max} \Lambda_E}{4\mathfrak{z}} \right)^2} - 1 \\ \mathfrak{z} &= \frac{-\mathbf{b} - \sqrt{\mathbf{b}^2 - 4\mathbf{a}\mathbf{c}}}{2\mathbf{a}} \\ \mathbf{a} &= \left(\frac{N_E - 1}{N - 1} J_{EE} \right)^2 - \frac{N_E N_I (N_E - 1)}{(N - 1)^2 (N_I - 1)} \frac{J_{EE} J_{EI} J_{IE}}{J_{II}} \\ \mathbf{b} &= -\frac{2}{\tau_E} \frac{N_E - 1}{N - 1} J_{EE} + \frac{N_E N_I}{(N - 1)(N_I - 1)} \frac{J_{EI} J_{IE}}{J_{II}} \left(\frac{1}{\tau_E} + \frac{1}{\tau_I} \right) \\ \mathbf{c} &= \frac{1}{\tau_E^2} \end{aligned} \quad (19)$$

Now, as we said, BT represents the point where the LP and H curves meet each other, and identifies also the end of the H curve. Clearly, from the condition $\lambda_0 = 0$ or $\lambda_1 = 0$ that defines the LP curves, and the condition $\lambda_{0,1} = \pm i\omega$ (where i represents the imaginary unit) that defines the H curves, we get $\lambda_0 = \lambda_1 = 0$. This is the condition that defines analytically the BT points, or equivalently $\mathbf{v}_{\text{BT}} = \mathbf{v}_{e,f}$ as given by Eq. (19), from which the coordinates of the BT points in the $I_E - I_I$ plane can be easily obtained through Eq. (5). The remaining local bifurcations (i.e. CP and GH) are analytically intractable, therefore we cannot study them beyond the numerical results.

To conclude this subsection, now we describe briefly the effect of the variation of the remaining synaptic weights on the codimension two bifurcation diagram, considering the weights in Tab. (1) as reference point. As we said, their variation does not generate interesting phenomena such as the branching point bifurcation which is obtained by varying J_{II} , so we dedicate less space to these parameters.

For $J_{EE} \gg 10$, the two LP curves become larger and larger on the I_E axis (i.e. the distance between their vertical asymptotes increases). Moreover, the curves get closer and closer to each other, by shifting on the I_E axis, until they intersect and their oblique parts (i.e. those between the BT points) overlap. If we increase J_{EE} further, the LP curves split again in two disjoint parts, each one presenting two BT and two CP bifurcations (so the total number of CP points increases from two to four). Between each pair of BT points (on the same LP curve) there is a H curve. These curves are very close to the corresponding LP curves, and if we increase J_{EE} further they disappear, together with the BT bifurcations. So for

very large J_{EE} we get only two disconnected LP curves, or in other terms for very strong excitation the oscillatory activity cannot be sustained anymore. Also on the opposite side, namely for weak inhibition (i.e. $J_{EE} \rightarrow 0$), the H curves disappear. Moreover, the width on the I_E axis of the LP curves decreases, i.e. the distance between their vertical asymptotes becomes smaller and smaller, until the asymptotes collapse on each other and the LP curves disappear as well.

For $|J_{EI}| \gg 70$, the width of the two LP curves remains almost constant, while the distance between them (and therefore also the length of the H curves) increases continuously. On the other side, for $|J_{EI}| \rightarrow 0$, the two LP curves get closer and closer to each other, until they intersect and then their oblique parts between the BT points overlap. If we decrease $|J_{EI}|$ further, similarly to the case with large J_{EE} , the two LP curves split in two disjoint parts, each one presenting two BT and two CP bifurcations. For even smaller values of $|J_{EI}|$, the BT, CP and H bifurcations disappear, while the LP curves disappear for $|J_{EI}| = 0$.

For $J_{IE} \gg 70$, the LP curves are stretched vertically and shifted downwards along the I_I axis. Clearly, in the opposite direction (i.e. for $J_{IE} \rightarrow 0$), they are compressed, and while the I_E coordinates of the vertical asymptotes remain almost unchanged with J_{IE} , the two CP points get closer and closer to each other. At the same time, the two H curves tend to overlap. At some value of J_{IE} , the two CP bifurcations touch each other and disappear, so the two LP curves become tangent. If we further decrease J_{IE} , the two LP curves split again, one over the other, and the BT and H bifurcations disappear.

All the phenomena that we have just described are qualitatively similar for different values of J_{II} , so they occur also in the strong-inhibition regime for the primary branch.

3.3 Strong-inhibition regime ($\lambda_I \geq 0$)

In the strong-inhibition regime (in particular here we consider the cases $J_{II} = -34$ and $J_{II} = -100$), most of the features of the weak-inhibition bifurcation diagram are preserved. However, besides the bifurcations explained in SubSec. (3.2), from Figs. (8), (9), (10), we can see that the system undergoes also the following codimension one bifurcations:

- local branching point bifurcations (BP), at which two or more equilibrium curves intersect each other;
- local torus bifurcations (TR), at which the limit cycles are characterized by a quasi-periodic motion;

and the following codimension two bifurcations:

- local zero-Hopf (neutral saddle) bifurcations (ZH), that involves the Andronov-Hopf curves and, in our case, the branching point curves. Around this point, both subcritical and supercritical Andronov-Hopf bifurcations exist.

In particular, the branching point bifurcations lead our model to show multiple branches of stationary solutions for suitable current values. This is a finite-size effect, due to the finite number of neurons in each population, that leads to a richer set of Jacobian matrix eigenvalues than that obtained by using methods based on the reduction of the number of equations, such as the mean-field approximation (see SubSec. (3.5) for more details). In order to thoroughly investigate the bifurcations the system undergoes in presence of strong inhibition, we start by analyzing the codimension one bifurcation diagram for $J_{II} = -34$. In particular, the diagram in Fig. (8) is obtained by letting $I_I = -10$. It turns out that, in addition to the primary equilibrium point curve (black line), new branches of stationary states (violet lines) emanate and collapse in two branching point bifurcations, BP. These secondary branches hold supercritical Andronov-Hopf bifurcations that give rise to stable limit cycles. Instead, on the primary branch, we find two saddle-node bifurcations and a subcritical Andronov-Hopf bifurcation, whose unstable limit cycles vanish in a homoclinic orbit. We remind that branching point bifurcations occur because λ_I changes sign. We also observe that for $N_I = 2$ the inhibitory neurons have the same bifurcation

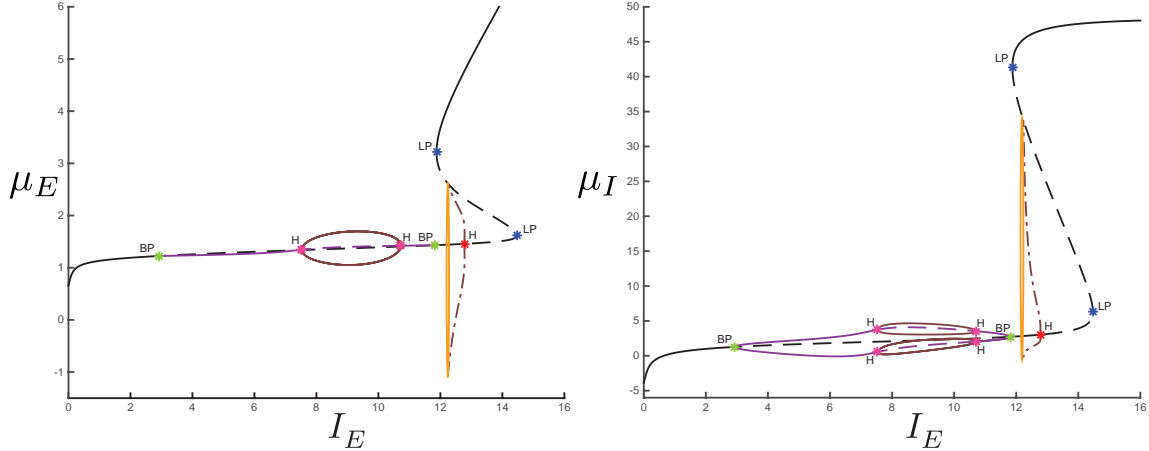


Figure 8: Codimension one bifurcation diagrams for μ_E (left) and μ_I (right) as a function of I_E , for $J_{II} = -34$ and $I_I = -10$. In both the graphs, the stable/unstable primary equilibrium curve is described by plain/dashed black curves, while the secondary ones are described by plain/dashed violet curves. Andronov-Hopf bifurcation appear on both the primary and secondary equilibrium curves, giving rise to unstable and stable limit cycles respectively. In particular, the unstable cycles collapse into a homoclinic bifurcation, described by an orange line.

diagram (see Fig. (8), right). However, this does not mean that the inhibitory membrane potentials are homogeneous. Indeed, when an inhibitory neuron is on the upper secondary branch (see the violet curve above the primary equilibrium point curve in Fig. (8), right), the other one is in the lower secondary branch, so indeed they are heterogeneous.

For $J_{II} = -100$, secondary branches of equilibrium points are still present, see Fig. (9). Together with a subcritical Andronov-Hopf bifurcation, they unveil also saddle-node ones. In particular, the former generates unstable limit cycles that become stable after having crossed the limit point of cycles bifurcation (dark green line). For increasing values of I_E , the stable limit cycles collapse into the unstable limit cycles originated from the subcritical Andronov-Hopf bifurcation belonging to the primary equilibrium point curve. Before collapsing, the stable limit cycles undergo torus bifurcations (gray line).

By varying also I_I , we obtain the codimension two bifurcation diagrams displayed in Fig. (10). It is worth noting that the branching points the system undergoes generate two bifurcation curves (light green lines) that pass through the whole $I_E - I_I$ domain. The presence of these curves is the most relevant difference with the weak-inhibition regime and the classic (mean-field) Wilson-Cowan model. Furthermore, the LP and H bifurcations that belong to the secondary branches give rise to further bifurcation curves (purple and light blue lines, respectively) in the $I_E - I_I$ domain, as shown in Fig. (10).

Interestingly, since the branching point bifurcation increases the dimension of the network from 2 (for $\lambda_I < 0$, see Eq. (5)) to 3 (for $\lambda_I > 0$, see Eq. (11)), the network can exhibit more complex dynamics, such as quasi-periodic motions originated from the torus bifurcations. The biological importance of quasi-periodic oscillations in neural communication was discussed in [57].

Now we want to study the local bifurcations from the analytical point of view. We start by considering the BP bifurcations, which are defined by the condition $\lambda_I = 0$, as we saw before. From Eq. (7) this condition implies:

$$\mathcal{A}'_I(\mu_I(\text{BP})) = \frac{N-1}{\tau_I |J_{II}|} \quad (20)$$

so the solutions of this equation are:

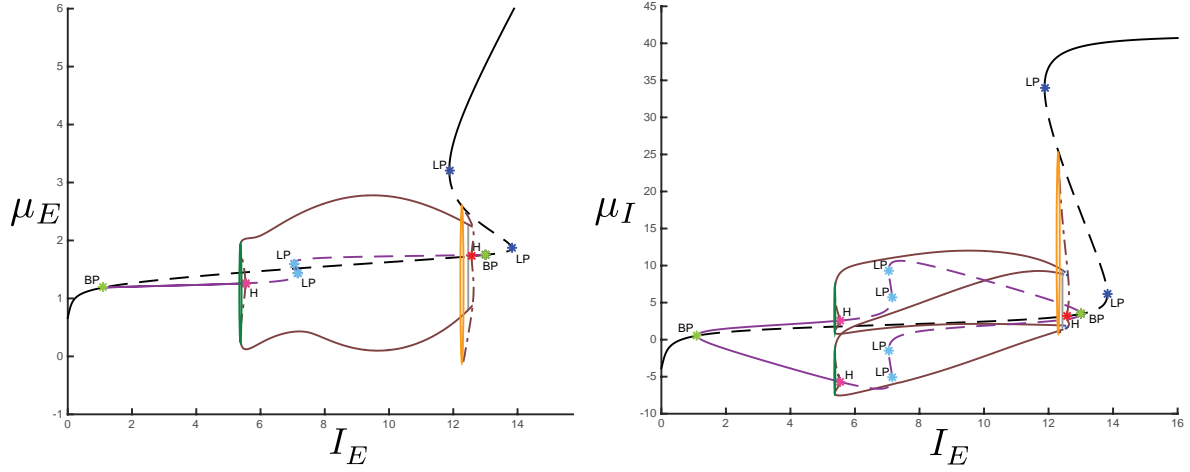


Figure 9: Codimension one bifurcation diagrams for μ_E (left) and μ_I (right) as a function of I_E , for $J_{II} = -100$ and $I_I = -10$. The colored curves describe the same bifurcations as in Fig. (8). Besides, we observe an LPC bifurcation (dark green line) and a TR bifurcation (gray line).

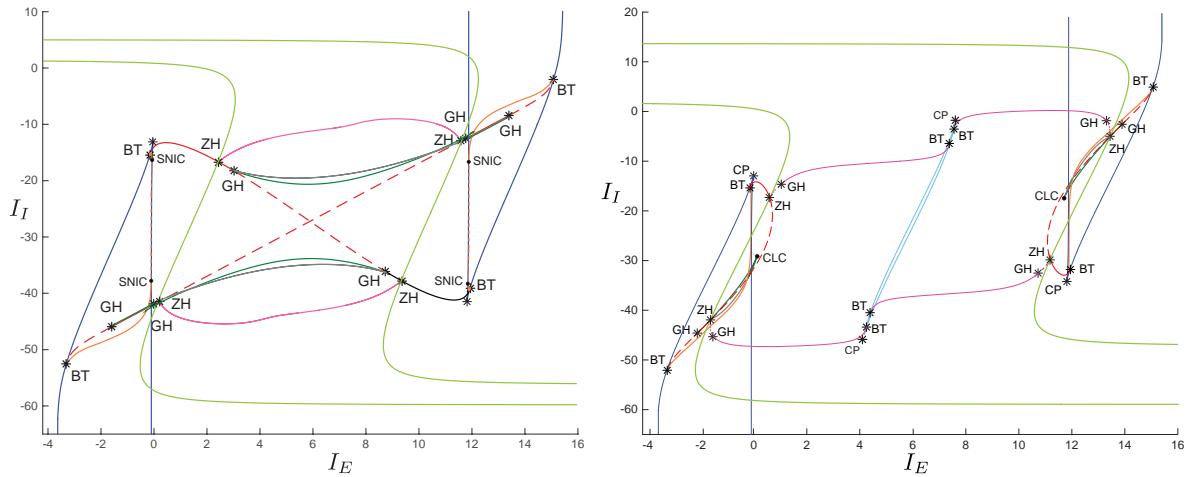


Figure 10: Codimension two bifurcation diagram on the $I_E - I_I$ plane for $J_{II} = -34$ (left) and $J_{II} = -100$ (right). In addition to the bifurcations already displayed in Fig. (7), we stress the presence of new ones. The branching points form two curves (light green lines), that define the values of $I_E - I_I$ that bound the secondary branches of equilibrium points (see the violet curves in Figs. (8) and (9)). The bifurcations originated on the secondary branches are differentiated from those originated on the primary one. Specifically, we show Andronov-Hopf and saddle-node curves (purple and light blue lines, respectively). In addition, we display the torus bifurcation curve (gray lines).

$$\mu_I(\text{BP}) = V_I^T \pm \frac{2}{\Lambda_I} \sqrt[3]{\sqrt{\left(\frac{\tau_I |J_{II}| \nu_I^{\max} \Lambda_I}{4(N-1)}\right)^2} - 1} \quad (21)$$

Now, from the second equation of the system (5) (we can also use Eq. (11), since for $\lambda_I = 0$ they are equivalent) we get:

$$\mu_E(\text{BP}) = V_E^T \pm \frac{2}{\Lambda_E} \sqrt{\frac{1}{\left\{ \frac{2(N-1)}{\nu_E^{\max} N_E J_{IE}} \left[\frac{1}{\tau_I} \mu_I(\text{BP}) - \frac{N_I-1}{N-1} J_{II} \mathcal{A}_I(\mu_I(\text{BP})) - I_I \right] - 1 \right\}^2} - 1}} \quad (22)$$

while from the first equation of (5) we get:

$$I_E = \frac{1}{\tau_E} \mu_E(\text{BP}) - \frac{N_E-1}{N-1} J_{EE} \mathcal{A}_E(\mu_E(\text{BP})) - \frac{N_I}{N-1} J_{EI} \mathcal{A}_I(\mu_I(\text{BP})) \quad (23)$$

where $\mu_I(\text{BP})$ and $\mu_E(\text{BP})$ are given by Eqs. (21) and (22) respectively. Since $\mu_E(\text{BP})$ depends on I_I , Eq. (23) defines two explicit functions $I_E = \mathcal{F}_{\pm}(I_I)$, that provide the curves on which we have a branching point bifurcation (see the light green lines in Fig. (10) for $J_{II} = -34$ and $J_{II} = -100$. More details can be found in SubSec. (S4.2.1) of the Supplementary Materials).

The points where the H and BP curves meet each other define the ZH bifurcation. From this definition, we see that they can be calculated analytically from the conditions $\lambda_{0,1} = \pm i\omega$ and $\lambda_I = 0$, from which in turn we get:

$$\mathcal{A}'_E(\mu_E(\text{ZH})) = \frac{N-1}{(N_E-1)J_{EE}} \left(\frac{1}{\tau_E} + \frac{N_I}{\tau_I} \right)$$

$$\mathcal{A}'_I(\mu_I(\text{ZH})) = \frac{N-1}{\tau_I |J_{II}|}$$

and therefore:

$$\mu_E^{\pm}(\text{ZH}) = V_E^T \pm \frac{2}{\Lambda_E} \sqrt[3]{\sqrt{\left(\frac{\nu_E^{\max} \Lambda_E (N_E-1) J_{EE}}{4(N-1) \left(\frac{1}{\tau_E} + \frac{N_I}{\tau_I}\right)}\right)^2} - 1}}$$

$$\mu_I^{\pm}(\text{ZH}) = V_I^T \pm \frac{2}{\Lambda_I} \sqrt[3]{\sqrt{\left(\frac{\nu_I^{\max} \Lambda_I \tau_I |J_{II}|}{4(N-1)}\right)^2} - 1}}$$

As usual, if we substitute these expressions of the membrane potentials in Eq. (5) or (11), we obtain the coordinates of the ZH points in the $I_E - I_I$ plane.

As we said, on the secondary branches that are generated by the branching points, new bifurcations can occur (in the case $N_I = 2$, see for example the LP and H bifurcations in Figs. (8) and (9), and the corresponding light blue and purple curves in Fig. (10)), also new branching points (for $N_I > 2$), from which tertiary branches emerge, and so on. To study them, according to bifurcation theory, we need the Jacobian matrix of the network on the secondary (tertiary, and so on) branches, as we will explain more clearly in Sec. (3.4). As usual, we focus on the case $N_I = 2$, therefore we can determine the local bifurcations on the secondary branches by means of Eq. (12).

Now we start with the LP bifurcations. We know that they are defined by the condition that one of the eigenvalues of (12) is equal to zero. From it, as explained in SubSec. (S4.2.3) of the Supplementary Materials, we obtain that:

$$\mathcal{A}'_E(\mu_E) = \frac{\dot{b}}{\dot{a}} \quad (24)$$

where:

$$\begin{aligned} \dot{a} &= \frac{1}{\tau_I^2} \frac{N_E - 1}{N - 1} J_{EE} + \frac{1}{\tau_I} \frac{N_E}{(N - 1)^2} J_{EI} J_{IE} [\mathcal{A}'_I(\mu_{I,0}) + \mathcal{A}'_I(\mu_{I,1})] \\ &\quad + \frac{1}{(N - 1)^3} [2N_E J_{EI} J_{IE} J_{II} - (N_E - 1) J_{EE} J_{II}^2] \mathcal{A}'_I(\mu_{I,0}) \mathcal{A}'_I(\mu_{I,1}) \\ \dot{b} &= \frac{1}{\tau_E} \left[\frac{1}{\tau_I^2} - \left(\frac{J_{II}}{N - 1} \right)^2 \mathcal{A}'_I(\mu_{I,0}) \mathcal{A}'_I(\mu_{I,1}) \right] \end{aligned}$$

So if we invert Eq. (24) and we use the solution of Eq. (13), we obtain the expression of μ_E as a function of $\mu_{I,0}$. If we replace the solutions μ_E and $\mu_{I,1}$ in the system (11), we get parametric equations for $I_{E,I}$ as a function of a single parameter, which is now defined as $\mathbf{v} \stackrel{\text{def}}{=} \mu_{I,0}$. These equations are an analytical description of the light blue curves shown in Fig. (10) (right) for $J_{II} = -100$.

Similarly, for the H bifurcations we obtain the condition:

$$\mathcal{A}'_E(\mu_E^\pm) = \frac{-\dot{b} \pm \sqrt{\dot{b}^2 - 4\dot{a}\dot{c}}}{2\dot{a}} \quad (25)$$

where:

$$\begin{aligned} \dot{a} &= \frac{N_E - 1}{N - 1} J_{EE} \left[\frac{2}{\tau_I} \frac{N_E - 1}{N - 1} J_{EE} + \frac{N_E}{(N - 1)^2} J_{EI} J_{IE} (\mathcal{A}'_I(\mu_{I,0}) + \mathcal{A}'_I(\mu_{I,1})) \right] \\ \dot{b} &= 2 \frac{N_E}{(N - 1)^3} J_{EI} J_{IE} J_{II} \mathcal{A}'_I(\mu_{I,0}) \mathcal{A}'_I(\mu_{I,1}) - \left(\frac{1}{\tau_E} + \frac{1}{\tau_I} \right) \left[\frac{4}{\tau_I} \frac{N_E - 1}{N - 1} J_{EE} + \frac{N_E}{(N - 1)^2} J_{EI} J_{IE} (\mathcal{A}'_I(\mu_{I,0}) + \mathcal{A}'_I(\mu_{I,1})) \right] \\ \dot{c} &= \frac{2}{\tau_I} \left[\left(\frac{1}{\tau_E} + \frac{1}{\tau_I} \right)^2 - \left(\frac{J_{II}}{N - 1} \right)^2 \mathcal{A}'_I(\mu_{I,0}) \mathcal{A}'_I(\mu_{I,1}) \right] \end{aligned}$$

so again it is possible to describe these bifurcations analytically, obtaining the same results we got numerically in Fig. (10) for $J_{II} = -34$ and $J_{II} = -100$ (see the purple curves in both the panels). However, unlike the primary branch, our theory does not allow us to calculate the range of the parameter $\mathbf{v} = \mu_{I,0}$ on the secondary branches, since the resulting equations that define the range are analytically intractable. In the same way, now it is not possible to calculate explicitly the coordinates of the new BT bifurcations, where the LP and H curves that emanate from the secondary branches meet each other. Therefore analytical approximations or numerical schemes must be used to evaluate them, but this is beyond the purpose of the article.

As we did for the weak-inhibition regime, we conclude this section by describing briefly the effect of the variation of the remaining synaptic weights. As we said at the end of SubSec. (3.2), all the variations that occur on the primary branch are qualitatively similar for different values of J_{II} . On the other side, now we want to analyze the behavior of the BP curves and of the bifurcations on the secondary branches. For $J_{II} = -100$ and increasing J_{EE} , the most notable phenomenon is the overlapping between the oblique parts of the BP and the LP curves of the primary branch. The latter finally collapse on each other and split in two disjoint parts as in the case $J_{II} = -10$ discussed in SubSec. (3.2), while the bifurcations on the secondary branches do not show any interesting variation. Furthermore, when $J_{EE} \rightarrow 0$, we observe first of all the disappearance of the ZH bifurcations. This occurs because the H curves on both the primary and the secondary branches do not meet the BP curve anymore. If we further decrease J_{EE} , the two CP bifurcations on the LP curve of the secondary branches get closer and closer until they annihilate each other and the curve disappears. Clearly this phenomenon implies also the disappearance of the BT bifurcations on the secondary branches. For smaller values of J_{EE} , the H curves on both the primary and secondary branches disappear, and finally also the LP curve on the primary branch (see SubSec. (3.2)) and the BP curve. To conclude, for large $|J_{EI}|$ or large J_{IE} , the LP curve on the secondary branches disappears again through the annihilation of its CP points (as explained above), while on the other side, when at least one of the two synaptic weights is small, we do not observe any interesting variation of the bifurcations on the secondary branches.

3.4 The case with generic N_I

The same analysis can be performed on networks with a generic number N_I of inhibitory neurons. When λ_I , as given by Eq. (7), goes to zero, we observe in general the formation of secondary branches from the primary one. This means that an inhibitory membrane potential becomes different from the others, so we can reinterpret the system as a network with an excitatory population with N_E neurons, and two inhibitory populations, one with one neuron, and the other with $N_I - 1$ neurons. Furthermore, when we change the current I_E (while keeping $\lambda_I > 0$) with I_I fixed, at some point one of the eigenvalues of the Jacobian matrix of the system (10) (see the Thm. (S1) of the Supplementary Materials for their analytical calculation) may go to zero, generating a new branching point on the secondary branches. In this case, we observe the formation of tertiary branches, so now one of the previous $N_I - 1$ identical inhibitory membrane potentials becomes different from the others, and so on.

In Fig. (11) we show an example of formation of secondary branches in the case $N_I = 4$, obtained as usual for the values of the parameters reported in Tab. (1). As the reader may easily see, there is now an important difference compared to the case $N_I = 2$. For a network with only two inhibitory neurons, Eq. (11) implies that they both have the same codimension one bifurcation diagram (see the right panels of Figs. (8) and (9)). This is just a special case, because in general, for $N_I > 2$, we observe a symmetry-breaking not only at the level of the inhibitory membrane potentials, but also at the level of the codimension one bifurcation diagram. Indeed, from Fig. (11) we see that one inhibitory neuron, which is chosen randomly by the system, has a different diagram compared to the others. This is another example of symmetry-breaking that occurs in the system, as an implicit consequence of Eq. (10) for $N_I > 2$.

It is important to underline that, even if the BP curve (23) is defined for every N_I , numerically we observe the formation of new branches only for N_I even. In principle this may be proved rigorously by the

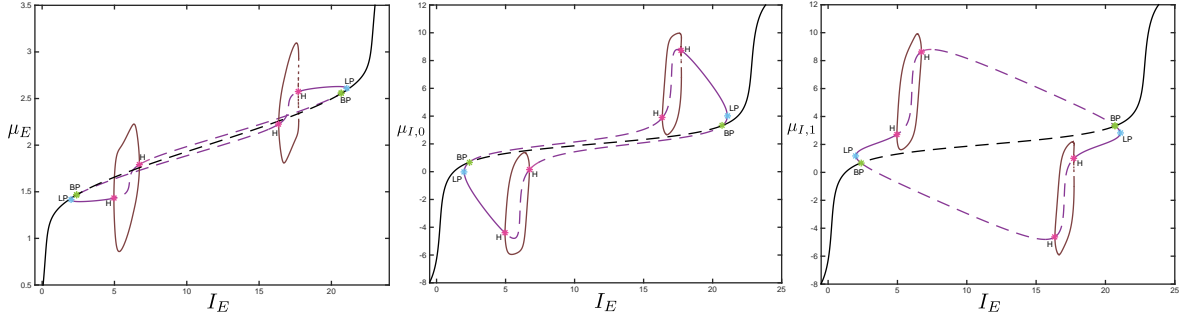


Figure 11: Codimension one bifurcation diagrams for $N_I = 4$. The left panel shows the diagram of the excitatory neurons, the central panel that of three of the inhibitory neurons, while the right panel shows the diagram of the remaining neuron in the inhibitory population. Interestingly, now the inhibitory neurons have not only different membrane potentials, but also different codimension one bifurcation diagrams. The neuron with the different diagram is chosen randomly by the system, so this is another example of symmetry-breaking that occurs in the network for strong inhibition.

so called *Lyapunov-Schmidt bifurcation equation* [58], but since the proof is rather technical and beyond the purpose of this article, we do not report it here.

For a generic N_I , local bifurcations can still be calculated analytically as we showed before. Indeed, from the second equation of (10), it is possible to express $N_I - 1$ inhibitory membrane potentials as functions of the remaining one, which can be used as a parameter for the parametric equations in the codimension two bifurcation diagram.

To conclude, we observe that now new kinds of bifurcations can appear, which do not occur in the case $N_I = 2$. For example, for $N_I = 4$, if the network has four different inhibitory potentials, the characteristic equation of the Jacobian matrix has the form $p(\lambda) = (\lambda - \lambda_E)^{N_E-1} p_R(\lambda)$, where $p_R(\lambda)$ (the characteristic polynomial of the reduced Jacobian matrix introduced in Thm. (S1) of the Supplementary Materials) is a fifth order polynomial. This means that in principle, for some values of the parameters, the network may have two pairs of purely imaginary eigenvalues. This condition corresponds to the formation of a so called *double-Hopf bifurcation*, which in turn may imply a local birth of *chaos* (e.g. [59, 60]). Indeed, for $\lambda_I > 0$ the dimension of the system is larger than 2 due to the BP bifurcations, therefore according to the Poincaré–Bendixson theorem the network may exhibit chaotic behavior.

3.5 Differences between our approach and the mean-field theory

In this section we explain in detail why the mean-field theory cannot describe the branching point bifurcation. Given the system (3), the mean-field theory makes the assumption that within each population the membrane potentials are independent and identically distributed. Therefore, by hypothesis, it forbids the presence of heterogeneous solutions, like those that emerge from the branching point bifurcation. Due to this assumption, Eq. (3) can be reduced to a system of two differential equations, according to the mean-field theory developed by Sznitman, Tanaka, McKean and others [61–68]:

$$\begin{cases} \frac{dV_E(t)}{dt} = \frac{1}{\tau_E} V_E(t) + R_E J_{EE} \mathbb{E}[\mathcal{A}_E(V_E(t))] + R_I J_{EI} \mathbb{E}[\mathcal{A}_I(V_I(t))] + I_E \\ \frac{dV_I(t)}{dt} = \frac{1}{\tau_I} V_I(t) + R_E J_{IE} \mathbb{E}[\mathcal{A}_E(V_E(t))] + R_I J_{II} \mathbb{E}[\mathcal{A}_I(V_I(t))] + I_I \end{cases} \quad (26)$$

where $R_\alpha = \lim_{N \rightarrow \infty} \frac{N_\alpha}{N}$ (namely the ratio between the population α and the whole network in the thermodynamic limit, so in our case $R_E = 0.8$ and $R_I = 0.2$), while V_α represents any membrane potential in the population α . Moreover, $\mathbb{E}[\cdot]$ denotes the average over trials at a given time instant, and it means that the system is generally supposed to be stochastic. Stochasticity can be introduced in different ways, for example through Brownian motions, random initial conditions, or random synaptic weights [17]. In this article we are considering a deterministic system, therefore we get simply $\mathbb{E}[\mathcal{A}_\alpha(V_\alpha(t))] = \mathcal{A}_\alpha(V_\alpha(t))$. In this way, the neural network is described by a system of two coupled equations in the unknowns $V_{E,I}(t)$, whose Jacobian matrix is:

$$\mathcal{J}^{\text{mf}} = \begin{bmatrix} -\frac{1}{\tau_E} + R_E J_{EE} \mathcal{A}'_E(\mu_E) & R_I J_{EI} \mathcal{A}'_I(\mu_I) \\ R_E J_{IE} \mathcal{A}'_E(\mu_E) & -\frac{1}{\tau_I} + R_I J_{II} \mathcal{A}'_I(\mu_I) \end{bmatrix} \quad (27)$$

Its characteristic equation is:

$$a^{\text{mf}} \left(\lambda_{0,1}^{\text{mf}} \right)^2 + b^{\text{mf}} \lambda_{0,1}^{\text{mf}} + c^{\text{mf}} = 0$$

where:

$$a^{\text{mf}} = 1$$

$$b^{\text{mf}} = \frac{1}{\tau_E} + \frac{1}{\tau_I} - R_E J_{EE} \mathcal{A}'_E(\mu_E) - R_I J_{II} \mathcal{A}'_I(\mu_I)$$

$$c^{\text{mf}} = \frac{1}{\tau_E \tau_I} - \left(\frac{1}{\tau_E} R_I J_{II} \mathcal{A}'_I(\mu_I) + \frac{1}{\tau_I} R_E J_{EE} \mathcal{A}'_E(\mu_E) \right) + R_E R_I (J_{EE} J_{II} - J_{IE} J_{EI}) \mathcal{A}'_E(\mu_E) \mathcal{A}'_I(\mu_I)$$

From Eq. (7) it is easy to see that $\lim_{N \rightarrow \infty} \lambda_{0,1} = \lambda_{0,1}^{\text{mf}}$. The only difference between $\lambda_{0,1}$ and $\lambda_{0,1}^{\text{mf}}$ is in the ratios that multiply the synaptic weights ($\frac{N_\alpha - 1}{N - 1}$ or $\frac{N_\alpha}{N - 1}$ for the finite-size network, and R_α in the mean-field case). This difference, due to the absence of self connections, is small for large networks. So in a sense, when compared to a finite-size network, the mean-field approximation takes into account only the information provided by $\lambda_{0,1}$, and neglects that of $\lambda_{E,I}$. Clearly λ_E is always negative, therefore it never affects the changes of dynamics of the system. However, in a finite-size network λ_I can change sign, generating a branching point bifurcation. The mean-field approximation neglects this information, and it can be seen as a consequence of the fact that $\lim_{N \rightarrow \infty} \lambda_I = -\frac{1}{\tau_I}$. In other words, in the thermodynamic limit the eigenvalue λ_I is always negative, therefore it cannot generate branching point bifurcations. In more mathematically rigorous terms, we get that the *center manifold* [26] of the network is not affected anymore by λ_I for $N \rightarrow \infty$, so that the dynamics is governed only by $\lambda_{0,1}$. This clearly proves that the mean-field approximation oversimplifies the description of the network, since it is able to describe only the primary branch.

3.6 Finite-size effects are stronger for biologically plausible anatomical connections

By comparing the right panels of Figs. (8) and (9), it is clear that the magnitude of the branching point finite-size effects is proportional to the magnitude of J_{II} . Indeed, from these figures we can see that,

for a given I_E , the difference between the membrane potentials of the primary and secondary branches increases with $|J_{II}|$. Moreover, from Fig. (10) we observe that for $J_{II} = -100$ the codimension two diagram is more complex than the case $J_{II} = -34$, due to the formation of LP, CP and BT bifurcations on the secondary branches. On the other side, in SubSec. (3.5) we have seen that the branching point bifurcations disappear in the thermodynamic limit. This is a consequence of the increasing number of incoming connections $M_I = N - 1$, which implies that $\lim_{N \rightarrow \infty} \lambda_I = -\frac{1}{\tau_I} < 0$. Therefore from all these observations we conclude that the magnitude of the finite size effects is related to the ratio $\frac{J_{II}}{M_I}$ in the formula of λ_I (see Eq. (7)). In other terms, both inhibition and the topology of the anatomical connections determine the strength of the finite-size effects. In particular, here we want to discuss the importance of the parameter M_I .

For this reason, we extend our analysis to the case of a more realistic connectivity matrix (to simplify matters, we consider a purely inhibitory neural network, since it is sufficient to show branching point bifurcations). For example, we can consider the block-circulant topology $\mathcal{BC}_{F,G}(\mathcal{M}_0, \dots, \mathcal{M}_{F-1})$ with circulant-band blocks introduced in [17]:

$$J = J_{II} \begin{bmatrix} \mathfrak{B}^{(0)} & \mathfrak{B}^{(1)} & \dots & \mathfrak{B}^{(F-1)} \\ \mathfrak{B}^{(F-1)} & \mathfrak{B}^{(0)} & \dots & \mathfrak{B}^{(F-2)} \\ \vdots & \vdots & \ddots & \vdots \\ \mathfrak{B}^{(1)} & \mathfrak{B}^{(2)} & \dots & \mathfrak{B}^{(0)} \end{bmatrix}, \quad (28)$$

$$\mathfrak{B}^{(i)} = \begin{bmatrix} 1 - \delta_{i0} & 1 & \dots & 1 & 0 & \dots & 0 & 1 & \dots & 1 \\ 1 & 1 - \delta_{i0} & \ddots & & \ddots & \ddots & & \ddots & \ddots & \vdots \\ \vdots & \ddots & \ddots & \ddots & & \ddots & \ddots & & \ddots & 1 \\ 1 & & \ddots & \ddots & \ddots & \ddots & \ddots & \ddots & & 0 \\ 0 & \ddots & & \ddots & \ddots & \ddots & \ddots & \ddots & & \vdots \\ \vdots & & \ddots & & \ddots & \ddots & \ddots & & \ddots & 0 \\ 0 & & & \ddots & & \ddots & \ddots & \ddots & & 1 \\ 1 & \ddots & & & \ddots & & \ddots & \ddots & \ddots & \vdots \\ \vdots & \ddots & \ddots & & \ddots & & \ddots & \ddots & 1 - \delta_{i0} & 1 \\ 1 & \dots & 1 & 0 & \dots & 0 & 1 & \dots & 1 & 1 - \delta_{i0} \end{bmatrix}$$

where $\mathfrak{B}^{(0)}, \dots, \mathfrak{B}^{(F-1)}$ are $G \times G$ circulant matrices (so that $FG = N$), with bandwidth $2\xi_i + 1$, for $i = 0, \dots, F - 1$. The network equipped with these synaptic connections can be interpreted as a collection of F neural masses with G neurons each. If we define:

$$H(x) = \begin{cases} 0, & x \leq 0 \\ 1, & x > 0 \end{cases}$$

then $\mathcal{M}_0 \stackrel{\text{def}}{=} 2\xi_0 - H\left(\xi_0 - \lfloor \frac{G}{2} \rfloor + (-1)^G\right)$ is the number of connections that every neuron in a given mass receives from the neurons in the same mass. Furthermore, $\mathcal{M}_i \stackrel{\text{def}}{=} 2\xi_i + 1 - H\left(\xi_i - \lfloor \frac{G}{2} \rfloor + (-1)^G\right)$, for $i = 1, \dots, F - 1$, is the number of connections that every neuron in the j th mass receives from

the neurons in the $(i + j)$ th mod F mass, for $j = 0, \dots, F - 1$. Therefore we conclude that $M_I = F - 1 + \sum_{i=0}^{F-1} \left[2\xi_i - H \left(\xi_i - \lfloor \frac{G}{2} \rfloor + (-1)^G \right) \right]$.

Now, if we suppose that the membrane potentials are homogeneous, the eigenvalues of the corresponding Jacobian matrix are:

$$\lambda_{mG+n} = \begin{cases} -\frac{1}{\tau} + \frac{J_{II}}{M_I} \left[F - 1 + \sum_{i=0}^{F-1} g(n, \xi_i, G) \right] \mathcal{A}'_I(\mu_I), & m = 0, \forall n \\ -\frac{1}{\tau} + \frac{J_{II}}{M_I} \left[-1 + \sum_{i=0}^{F-1} e^{\frac{2\pi}{F} mi} g(n, \xi_i, G) \right] \mathcal{A}'_I(\mu_I), & m \neq 0, \forall n \end{cases} \quad (29)$$

$$g(n, \xi_i, G) = \begin{cases} 2\xi_i - H \left(\xi_i - \lfloor \frac{G}{2} \rfloor + (-1)^G \right), & n = 0, \forall \xi_i \\ -1, & n \neq 0, \xi_i = \lfloor \frac{G}{2} \rfloor \\ \frac{\sin \left(\frac{\pi n (2\xi_i + 1)}{G} \right)}{\sin \left(\frac{\pi n}{G} \right)} - 1, & n \neq 0, \xi_i < \lfloor \frac{G}{2} \rfloor \end{cases}$$

with $m = 0, \dots, F - 1$ and $n = 0, \dots, G - 1$. They depend on the ratio $\frac{J_{II}}{M_I}$, where M_I does not necessarily diverge in the thermodynamic limit (consider for example the case when $G \rightarrow \infty$ for F fixed, and the parameters ξ_i are finite and independent from G). Therefore, for N large enough, this topology exhibits stronger finite-size effects than the fully connected network.

To conclude, we also underline that, according to [17], if M_I does not diverge for $N \rightarrow \infty$, the neurons do not become independent, therefore Sznitman's mean-field theory cannot be used to simplify the description of the network. Moreover, from (29) we see that many of the eigenvalues λ_{mG+n} are distinct, since the reduced number of connections breaks the degeneracy of the system (compared to the fully-connected network, where λ_I has algebraic multiplicity $N_I - 1$). For this reason we argue that they generate a multitude of branching point bifurcations, not just two as in the fully-connected case, making plausible connections even more interesting from the biological and mathematical point of view.

4 Discussion

We proved the emergence of complex dynamics in small neural circuits, characterized by strong finite-size effects, that cannot be accounted for by the mean-field approximation. We showed, through a detailed numerical and analytical analysis of the bifurcations, that small symmetric neural networks undergo branching point bifurcations through spontaneous symmetry-breaking, that leads to the formation of strongly heterogeneous membrane potentials in the inhibitory population. This result is obtained when we increase the strength of the synaptic weights in the inhibitory population, and clearly falsifies the mean-field hypothesis of identically distributed neurons. This is a very interesting feature of our model, since from the simple assumption of identical neurons, it is able to exhibit heterogeneous membrane potentials, as in real networks.

From a biological point of view, strong inhibition may correspond to anesthetized neurons, since it was proved that some kinds of anesthetics, such as propofol, thiopental and isoflurane, act on γ -Aminobutyric acid (GABA), the primary inhibitory neurotransmitter in the brain [69]. Our results prove that the dynamics repertoire of neural populations can be completely different when the brain is under the influence of drugs, with important consequences on experiments with anesthetized animals. They also

underline the importance of the synaptic weights in determining the dynamical behavior of the neural network. As in the theory of hallucinations of Ermentrout and Cowan [28], the spontaneous symmetry-breaking is caused by drugs that increase the strength of the synaptic weights and generate alternative neural patterns. However, it is important to observe that while in their theory the network undergoes a symmetry-breaking through an increase of the excitatory weights, in our model symmetry is broken by an increase of the inhibitory ones.

The analysis we performed can be used to understand not only the dynamics of neural masses at the mesoscopic scale in big animals, but also the behavior of tiny brains such as those of rotifers and nematodes. However, it is important to observe that in this article we restricted the bifurcation analysis to small neural circuits, because of our hypothesis of all-to-all synaptic connectivity between neurons. This hypothesis allowed us to reduce the complexity of the analytical formulas, but predicted that the magnitude of the finite size-effects is inversely proportional to the number of incoming connections per neuron, that for a fully connected topology is proportional to the network's size. Therefore, after relaxing the hypothesis of all-to-all connectivity, in order to study the behavior of biologically more plausible networks, we argued the formation of multiple branching point bifurcations and a stronger heterogeneity of the membrane potentials, as a consequence of the reduced number of synaptic connections. This means that in principle strong finite-size effects can occur also in large networks, if their anatomical connections are sufficiently sparse.

We also observe that our study may be extended to gain some insights into the oscillations that emerge from Hopf bifurcations. In the codimension one bifurcation diagram, when the current I_E is close to the one that generates a Hopf bifurcation, the amplitude of the oscillation that appears from the H point is small. For this reason, the solution of the system (3) can be approximated by a truncated Fourier series. Semi-analytical expressions of the amplitudes of the harmonics can be obtained by applying the so called *harmonic balance methods*, which were developed especially in the context of electrical engineering [70]. In principle, these tools may be used to study the formation of torus bifurcations and eventually the transition to chaos [71–74].

Furthermore, we stress the fact that the analytical study of local bifurcations introduced in our work can be easily extended to neural networks composed of several populations, by means of the Thm. (S1) reported in the Supplementary Materials. In this way we can shed new light on the behavior of more complex and biologically plausible networks, also when numerical simulations become prohibitive. So for example we may think to extend our model to describe the interaction between six neural populations. These can be thought as a coarse description of the six layers of the cerebral cortex, therefore this system can be interpreted a simplified model of a cortical column. In general we obtain that in a network with \mathfrak{P} populations, a codimension \mathcal{C} bifurcation is described by a $(\mathfrak{P} - \mathcal{C})$ -dimensional manifold, whose parametric equations contain $\mathfrak{P} - \mathcal{C}$ independent parameters. The only exception, as in the case with two populations considered in this article, is the BP manifold, whose equation can be written by expressing any current as an explicit function of all the others (see Eqs. (21) + (22) + (23)). So for example, in a network with three populations A, B, C , in the codimension three diagram spanned by the currents I_A, I_B, I_C we get that:

- the bifurcations LP, H etc are described by surfaces with two parameters;
- BT, CP etc by lines with one parameter;
- codimension three bifurcations by points;
- the BP bifurcations are described by surfaces with explicit formulas $I_A = \mathcal{F}(I_B, I_C)$.

However, it is important to observe that a complete classification of bifurcations with $\mathcal{C} \geq 3$ is still missing in the literature, due to their complexity. Nevertheless the method introduced in this article in principle can be used to describe analytically some of them for any \mathcal{C} .

We underline that the Thm. (S1) can be used to describe also networks of interconnected neural masses (where each one is described by the system in Fig. 1). Interestingly, in the special case when the masses are identical, the symmetry group is more complex than that of a single mass. As we proved, we may observe spontaneous symmetry-breaking *within* a mass, through branching point bifurcations. However, since a network of masses has a larger symmetry, now symmetry-breaking can occur also *between* masses, which means that masses can behave differently even if they are identical. We found that in each mass the inhibitory membrane potentials can oscillate in synchrony or out of synchrony (on the primary and secondary branches, respectively). So in principle we may observe the formation of particular patterns of activity known as *chimera states* [75], where inhibitory neurons in one mass are synchronized while those in the other are not, even if the two masses are described by identical neural equations.

To conclude, we observe that our model can be extended and generalized in many other ways, through the introduction of delays, stochasticity, synaptic plasticity and more realistic topologies. All these additions allow us to improve the biological plausibility of the model, without losing the possibility to investigate analytically the complexity of its dynamics.

Acknowledgments

DF and AC were supported by the Autonomous Province of Trento, Call “Grandi Progetti 2012,” project “Characterizing and improving brain mechanisms of attention—ATTEND”.

SP was supported by the SI-CODE project of the Future and Emerging Technologies (FET) programme within the Seventh Framework Programme for Research of the European Commission, under FET-Open grant no. FP7-284553, and by the Autonomous Province of Trento, Call “Grandi Progetti 2012,” project “Characterizing and improving brain mechanisms of attention—ATTEND”.

We would like to thank Fabio Della Rossa from the department of Electronics, Information and Bioengineering of Politecnico di Milano (Italy), for providing some useful hints about Cl_MatCont.

The funders had no role in study design, data collection and analysis, decision to publish, interpretation of results, or preparation of the manuscript.

References

- [1] O. Sporns. Small-world connectivity, motif composition and complexity of fractal neuronal connections. *Biosystems*, **85**:55–64, 2006.
- [2] L. Ingber. Generic mesoscopic neural networks based on statistical mechanics of neocortical interactions. *Phys. Rev. A*, **45**(4):R2183–R2186, 1992.
- [3] W. J. Freeman. *Neurodynamics: An exploration in mesoscopic brain dynamics*. Springer-Verlag, London, 2000.
- [4] W. J. Freeman. Mesoscopic neurodynamics: From neuron to brain. *J. Physiol.*, **94**:303–322, 2000.
- [5] J. J. Wright, C. J. Rennie, G. J. Lees, P. A. Robinson, P. D. Bourke, C. L. Chapman, E. Gordon, and D. L. Rowe. Simulated electrocortical activity at microscopic, mesoscopic, and global scales. *Neuropsychopharmacol.*, **28**(Suppl. 1):S80–S93, 2003.
- [6] J. W. Bohland et al. A proposal for a coordinated effort for the determination of brainwide neuroanatomical connectivity in model organisms at a mesoscopic scale. *PLoS Comput. Biol.*, **5**:e1000334, 2009.

- [7] F. Grimbert. *Mesoscopic models of cortical structures*. PhD thesis, Univ. of Nice-Sophia Antipolis, 2008.
- [8] G. Deco, V. K. Jirsa, P. A. Robinson, M. Breakspear, and K. Friston. The dynamic brain: From spiking neurons to neural masses and cortical fields. *PLoS Comput. Biol.*, **4**:e1000092, 2008.
- [9] B. H. Jansen, G. Zouridakis, and M. E. Brandt. A neurophysiologically-based mathematical model of flash visual evoked potentials. *Biol. Cybern.*, **68**:275–283, 1993.
- [10] B. Jansen and V. Rit. Electroencephalogram and visual evoked potential generation in a mathematical model of coupled cortical columns. *Biol. Cybern.*, **73**:357–366, 1995.
- [11] A. Babajani and H. Soltanian-Zadeh. Integrated MEG/EEG and fMRI model based on neural masses. *IEEE Trans. Biomed. Eng.*, **53**:1794–1801, 2006.
- [12] O. Faugeras, J. Touboul, and B. Cessac. A constructive mean-field analysis of multi-population neural networks with random synaptic weights and stochastic inputs. *Front. Comput. Neurosci.*, **3**:1, 2009.
- [13] M. Samuelides and B. Cessac. Random recurrent neural networks dynamics. *Eur. Phys. J.-Spec. Top.*, **142**(1):89–122, 2007.
- [14] J. Baladron, D. Fasoli, O. Faugeras, and J. Touboul. Mean-field description and propagation of chaos in networks of Hodgkin-Huxley and FitzHugh-Nagumo neurons. *JMN*, **2**(1):10, 2012.
- [15] J. Touboul, G. Hermann, and O. Faugeras. Noise-induced behaviors in neural mean field dynamics. *SIAM J. Appl. Dyn. Syst.*, **11**(1):49–81, 2012.
- [16] B. Cessac. Increase in complexity in random neural networks. *J. Phys. I (France)*, **5**:409–432, 1995.
- [17] D. Fasoli, O. Faugeras, and S. Panzeri. A formalism for evaluating analytically the cross-correlation structure of a firing-rate network model. *JMN*, **5**:6, 2015.
- [18] P. Bressloff. Stochastic neural field theory and the system-size expansion. *SIAM J. Appl. Math.*, **70**(5):1488–1521, 2010.
- [19] M. A. Buice and C. C. Chow. Dynamic finite size effects in spiking neural networks. *PLoS Comput. Biol.*, **9**(1):e1002872, 2013.
- [20] O. Faugeras and J. MacLaurin. A large deviation principle for networks of rate neurons with correlated synaptic weights. *BMC Neurosci.*, **14**(Suppl. 1):252, 2013.
- [21] P. Bressloff. Path-integral methods for analyzing the effects of fluctuations in stochastic hybrid neural networks. *JMN*, **5**:4, 2015.
- [22] V. B. Mountcastle. The columnar organization of the neocortex. *Brain*, **120**:701–722, 1997.
- [23] D. P. Buxhoeveden and M. F. Casanova. The minicolumn hypothesis in neuroscience. *Brain*, **125**:935–951, 2002.
- [24] O. Sporns, G. Tononi, and R. Kötter. The human connectome: A structural description of the human brain. *PLoS Comput. Biol.*, **1**:e42, 2005.
- [25] R. D. Beer. On the dynamics of small continuous-time recurrent neural networks. *Adapt. Behav.*, **3**(4):469–509, 1995.

- [26] Y. A. Kuznetsov. *Elements of applied bifurcation theory*, Vol. 112. Springer-Verlag New York, 1998.
- [27] M. Golubitsky, I. Stewart, and D. G. Schaeffer. *Singularities and groups in bifurcation theory II, Vol. 69 of Appl. Math. Sci.*. Springer-Verlag New York, 2012.
- [28] G. B. Ermentrout and J. D. Cowan. A mathematical theory of visual hallucination patterns. *Biol. Cybernet.*, **34**:137–150, 1979.
- [29] J. Cohen and I. Stewart. *Polymorphism viewed as phenotypic symmetry-breaking*. In *Nonlinear Phenomena in Physical and Biological Sciences* (S. K. Malik, M. K. Chandrashekar and N. Pradhan eds.), New Delhi: Indian National Science Academy, 1–67, 2000.
- [30] I. Stewart, T. Elmhirst, and J. Cohen. *Symmetry-breaking as an origin of species*. In *Conference on Bifurcations, Symmetry, and Patterns* (J. Buescu, S. B. S. D. Castro, A. P. S. Dias and I. S. Laboriau eds.), Birkhäuser, Basel, 3–54, 2003.
- [31] A. P. S. Dias and I. Stewart. Secondary bifurcations in systems with all-to-all coupling. *Proc. R. Soc. Lond. A*, **459**:1969–1986, 2003.
- [32] T. Elmhirst. SN-equivariant symmetry-breaking bifurcations. *Int. J. Bifurcation Chaos Appl. Sci. Eng.*, **14**:1017–1036, 2004.
- [33] J. J. Hopfield. Neurons with graded response have collective computational properties like those of two-state neurons. *PNAS*, **81**(10):3088–3092, 1984.
- [34] H. R. Wilson and J. D. Cowan. Excitatory and inhibitory interactions in localized populations of model neurons. *Biophys J.*, **12**(1):1–24, 1972.
- [35] K. Engelborghs, T. Luzyanina, and D. Roose. Numerical bifurcation analysis of delay differential equations using DDE-BIFTOOL. *ACM Trans. Math. Software*, **28**(1):1–21, 2002.
- [36] S. Yi and A. G. Ulsoy. Solution of a system of linear delay differential equations using the matrix Lambert function. *Proc. Am. Control Conf.*, pages 2433–2438, 2006.
- [37] M. N. Shadlen and W. T. Newsome. Noise, neural codes and cortical organization. *Curr. Opin. Neurobiol.*, **4**:569–579, 1994.
- [38] W. Gerstner, A. Kreiter, H. Markram, and A. Herz. Neural codes: Firing rates and beyond. *Proc. Natl. Acad. Sci. USA*, **94**:12740–12741, 1997.
- [39] E. Salinas, H. Hernández, A. Zainos, and R. Romo. Periodicity and firing rate as candidate neural codes for the frequency of vibrotactile stimuli. *J. Neurosci.*, **20**:5503–5515, 2000.
- [40] S. Panzeri, N. Brunel, N. K. Logothetis, and C. Kayser. Sensory neural codes using multiplexed temporal scales. *Trends Neurosci.*, **33**:111–120, 2010.
- [41] S. R. Campbell and D. L. Wang. Synchronization and desynchronization in a network of locally coupled Wilson-Cowan oscillators. *IEEE Trans. Neural Netw.*, **7**(3):541–554, 1996.
- [42] D. Hansel and H. Sompolinsky. *Modeling feature selectivity in local cortical circuits, Chap. 13*. MIT Press, 1998.
- [43] E. Ledoux and N. Brunel. Dynamics of networks of excitatory and inhibitory neurons in response to time-dependent inputs. *Front. Comput. Neurosci.*, **5**:25, 2011.

- [44] H. Markram, M. Toledo-Rodriguez, Y. Wang, A. Gupta, G. Silberberg, and C. Wu. Interneurons of the neocortical inhibitory system. *Nat. Rev. Neurosci.*, **5**(10):793–807, 2004.
- [45] A. Dhooge, W. Govaerts, and Y. A. Kuznetsov. Matcont: A Matlab package for numerical bifurcation analysis of odes. *ACM TOMS*, **29**:141–164, 2003.
- [46] B. Ermentrout. *Simulating, analyzing, and animating dynamical systems: A guide to XPPAUT for researchers and students*. SIAM, Philadelphia, PA, USA, 2002.
- [47] S. H. Strogatz. *Nonlinear dynamics and chaos*. Sarat Book House, 1994.
- [48] B. G. Cragg and H. N. V. Temperley. Memory: The analogy with ferro-magnetic hysteresis. *Brain*, **78**(2):304–315, 1955.
- [49] L. Ingber. Statistical mechanics of neocortical interactions. Derivation of short-term-memory capacity. *Phys. Rev. A*, **29**(6):3346–3358, 1984.
- [50] X. J. Wang. Synaptic reverberation underlying mnemonic persistent activity. *Trends Neurosci.*, **24**(8):455–463, 2001.
- [51] L. M. Ward. Synchronous neural oscillations and cognitive processes. *Trends Cogn. Sci.*, **7**:553–559, 2003.
- [52] F. Hoppensteadt and E. M. Izhikevich. *Weakly connected neural networks*. Springer-Verlag New York, 1997.
- [53] E. C. Zeeman. Catastrophe theory. *Sci. Am.*, **234**:65–83, 1976.
- [54] P. Simen, F. Balci, L. de Souza, J. D. Cohen, and P. Holmes. A model of interval timing by neural integration. *J. Neurosci.*, **31**:9238–9253, 2011.
- [55] P. Simen. Evidence accumulator or decision threshold - Which cortical mechanism are we observing? *Front. Psychol.*, **3**:183 doi:10.3389/fpsyg.2012.00183, 2012.
- [56] L. G. Allan. The perception of time. *Percept. Psychophys.*, **26**:340–354, 1979.
- [57] E. M. Izhikevich. Weakly connected quasiperiodic oscillators, FM interactions, and multiplexing in the brain. *SIAM J. Appl. Math.*, **59**:2193–2223, 1999.
- [58] N. Sidorov, B. Loginov, A. Sinitsyn, and M. Falaleev. *Lyapunov-Schmidt methods in nonlinear analysis and applications*. Kluwer Academic Publishers, Dordrecht, 2002.
- [59] Q. Bi and P. Yu. Double Hopf bifurcations and chaos of a nonlinear vibration system. *Nonlinear Dynam.*, **19**:313–332, 1999.
- [60] P. Yu, Y. Yuan, and J. Xu. Study of double Hopf bifurcation and chaos for an oscillator with time delayed feedback. *Commun. Nonlinear Sci. Numer. Simul.*, **7**:69–91, 2002.
- [61] A. Sznitman. Nonlinear reflecting diffusion process, and the propagation of chaos and fluctuations associated. *J. Funct. Anal.*, **56**:311–336, 1984.
- [62] A. Sznitman. A propagation of chaos result for Burgers’ equation. *Prob. Theory Rel. Fields*, **71**:581–613, 1986.
- [63] A. Sznitman. Topics in propagation of chaos. In P.-L. Hennequin ed., *ecole d’été de probabilités de Saint-Flour XIX - 1989, Vol. 1464 of Lect. Notes Math., Chap. 3, pages 165–251*. Springer Berlin Heidelberg, 1991.

- [64] H. Tanaka. Probabilistic treatment of the Boltzmann equation of Maxwellian molecules. *Prob. Theory Rel. Fields*, **46**:67–105, 1978.
- [65] H. Tanaka. Central limit theorem for a simple diffusion model of interacting particles. *Hiroshima Math. J.*, **11**(2):415–423, 1981.
- [66] H. Tanaka. Some probabilistic problems in the spatially homogeneous Boltzmann equation. *Theory and Application of Random Fields (Lect. Notes Contr. Inf. Sci.)*, **49**:258–267, 1983.
- [67] H. McKean. A Class of Markov processes associated with nonlinear parabolic equations. *PNAS*, **56**(6):1907–1911, 1966.
- [68] H. McKean. Propagation of chaos for a class of non-linear parabolic equations. *In Stochastic Differential Equations (Lect. Ser. Differ. Eq., 7, Catholic Univ., 1967)*, pages 41–57. AFOSR, Arlington, Virginia, 1967.
- [69] P. S. Garcia, S. E. Kolesky, and A. Jenkins. General anesthetic actions on GABA(A) receptors. *Curr. Neuropharmacol.*, **8**:2–9, 2010.
- [70] A. I. Mees and L. O. Chua. The Hopf bifurcation theorem and its applications to nonlinear oscillations in circuits and systems. *IEEE Trans. Circuits Syst.*, **26**:235–254, 1979.
- [71] R. Genesio and A. Tesi. Harmonic balance methods for the analysis of chaotic dynamics in nonlinear systems. *Automatica*, **28**:531–548, 1992.
- [72] A. Tesi, E. H. Abed, R. Genesio, and H. O. Wang. Harmonic balance analysis of period-doubling bifurcations with implications for control of nonlinear dynamics. *Automatica*, **32**:1255–1271, 1996.
- [73] G. R. Itovich and J. L. Moiola. Double Hopf bifurcation analysis using frequency domain methods. *Nonlinear Dynam.*, **39**:235–258, 2005.
- [74] G. R. Itovich and J. L. Moiola. On period doubling bifurcations of cycles and the harmonic balance method. *Chaos Soliton Fract.*, **27**:647–665, 2006.
- [75] D. M. Abrams and S. H. Strogatz. Chimera states for coupled oscillators. *Phys. Rev. Lett.*, **93**:174102, 2004.